Marine and Petroleum Geology 162 (2024) 106753

Contents lists available at ScienceDirect

Marine and Petroleum Geology

journal homepage: www.elsevier.com/locate/marpetgeo

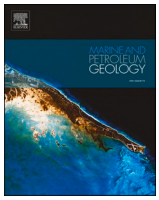

Zanclean to gelasian high-frequency sequences of the crotone basin (southern Italy): Architectural variability and forcing mechanisms

Massimo Zecchin [a,*], Mauro Caffau [a], Octavian Catuneanu [b]

[a] National Institute of Oceanography and Applied Geophysics - OGS, 34010, Sgonico, TS, Italy
[b] Department of Earth and Atmospheric Sciences, University of Alberta, 1-26 Earth Sciences Building, Edmonton, Alberta, T6G 2E3, Canada

ARTICLE INFO

Keywords:
Crotone basin
Belvedere formation
Strongoli sandstone
High-frequency sequences
Orbital forcing

ABSTRACT

The Zanclean Belvedere Formation and the Gelasian Strongoli Sandstone, cropping out in the Neogene to Quaternary Crotone Basin, southern Italy, exhibit a high-frequency cyclicity consisting of 10^{0}–10^{1} m sequences, which stack in an aggradational to progradational pattern. These high-frequency sequences are bounded by ravinement surfaces and are usually composed of transgressive and regressive deposits of similar thickness. In particular, the high-frequency sequences of the Belvedere Formation are composed of a transgressive systems tract and of a highstand systems tract, whereas those of the Strongoli Sandstone likely record also forced regression in their upper part. Due to the vertical repetition of the studied high-frequency sequences and their similar architecture despite the different tectonic settings in which the two formations accumulated, a climatic/glacio-eustatic control associated with earth-orbital parameters is very likely, as also documented in coeval successions worldwide. This contribution refines the correlation between shallow-marine sequences and their deep-water counterparts, which preserve a better record of the Milankovitch cyclicity.

1. Introduction

High-frequency sequences are stratigraphic cycles controlled by relative sea-level and/or sediment supply changes within the realm of fourth-order or lower rank stratigraphic frameworks (10^{2}–10^{5} yrs; Zecchin and Catuneanu, 2013; Catuneanu, 2019, 2022) and are very common in the Neogene and Quaternary sedimentary record (e.g., Naish and Kamp, 1997a,b; Saul et al., 1999; Massari et al., 2002; Di Celma et al., 2005; Zecchin et al., 2017, 2021, 2022). High-frequency sequences can exhibit variable stratigraphic architectures depending on the main forcing mechanisms governing their development (Zecchin, 2007; Catuneanu and Zecchin, 2013; Zecchin and Catuneanu, 2013). Being usually stacked to compose larger-scale cyclical successions, Neogene to Quaternary high-frequency sequences are commonly controlled by the Milankovitch orbital cyclicity, which was well documented in the deep-water record (e.g., Hilgen and Langereis, 1989; Hilgen, 1991; Ochoa et al., 2018). Although the correlation between shallow- and deep-water successions is often difficult due to the problematic dating of relatively coarse-grained proximal deposits, the control exerted by orbital forcing on shallow-water high-frequency sequences was demonstrated by several authors (e.g., Naish and Kamp, 1997a; Massari et al., 2002; Zecchin et al., 2016). The advantage of studying shallow-water high-frequency sequences controlled by the Milankovitch cyclicity, as opposed to cycles found in the deep-water record, is the possibility to recognize relative sea-level changes and/or sediment supply variations based on sequence stratigraphic principles. The possibility to link relatively proximal cyclic successions with their deep-water counterparts represents, therefore, a powerful tool to reconstruct the history of sedimentary basins and correlate global events.

This study deals with meter-to decameter-scale high-frequency sequences composing cyclic Zanclean and Gelasian successions of the Crotone Basin, southern Italy (Fig. 1). This Neogene to Quaternary basin has already been proven suitable to study the shallow-water high-frequency cyclicity and its controlling factors. Previous studies on these successions highlighted the general architecture of high-frequency sequences and established methods for recognizing ravinement surfaces, maximum flooding surfaces and bedset boundaries (Zecchin, 2005; Zecchin et al., 2017, 2021, 2022). In the present study, a comparison between Zanclean and the less known Gelasian high-frequency sequences of the Crotone Basin is made by selecting representative sections. The stratigraphic architecture of these sequences, as well as the

* Corresponding author.
E-mail address: mzecchin@ogs.it (M. Zecchin).

https://doi.org/10.1016/j.marpetgeo.2024.106753
Received 17 January 2024; Received in revised form 9 February 2024; Accepted 10 February 2024
Available online 12 February 2024

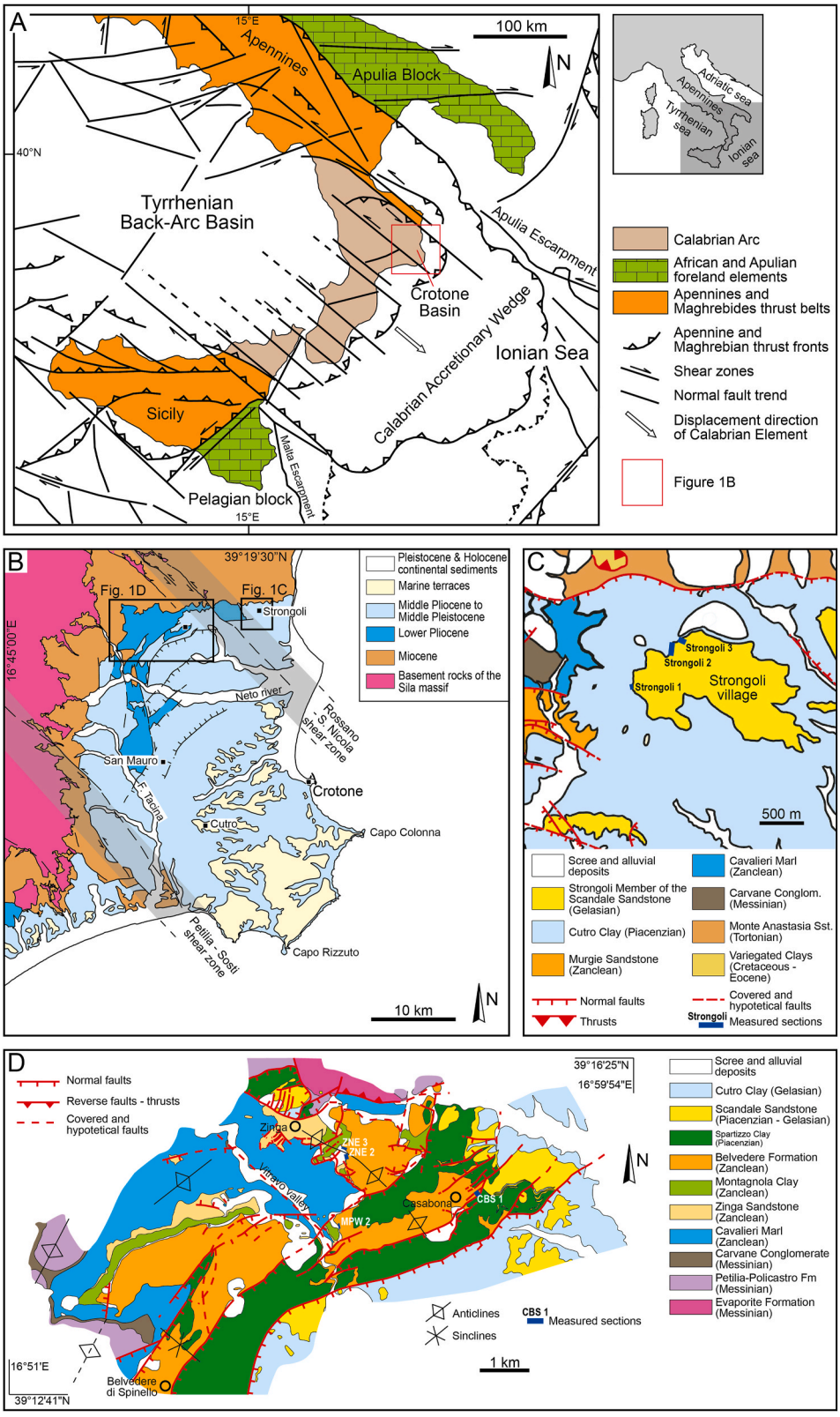

Fig. 1. (A) Structural map of the Calabrian Arc and location of the Crotone Basin (modified from Van Dijk and Okkes, 1991). (B) Simplified geological map of the Crotone Basin, reporting the position of the geologic maps shown in Fig. 1C and D (modified from Zecchin et al., 2004, 2021, 2022). (C) Geological map of the Strongoli area (Fig. 1B for location), showing the position of the Strongoli 1–3 measured sections (modified from Zecchin et al., 2020, 2022). (D) Geological map of the western part of the study area in the Crotone Basin (Fig. 1B for location), showing the position of the CBS 1, MPW 2, ZNE 2 and ZNE 3 measured sections (modified from Zecchin, 2005; Zecchin et al., 2021).

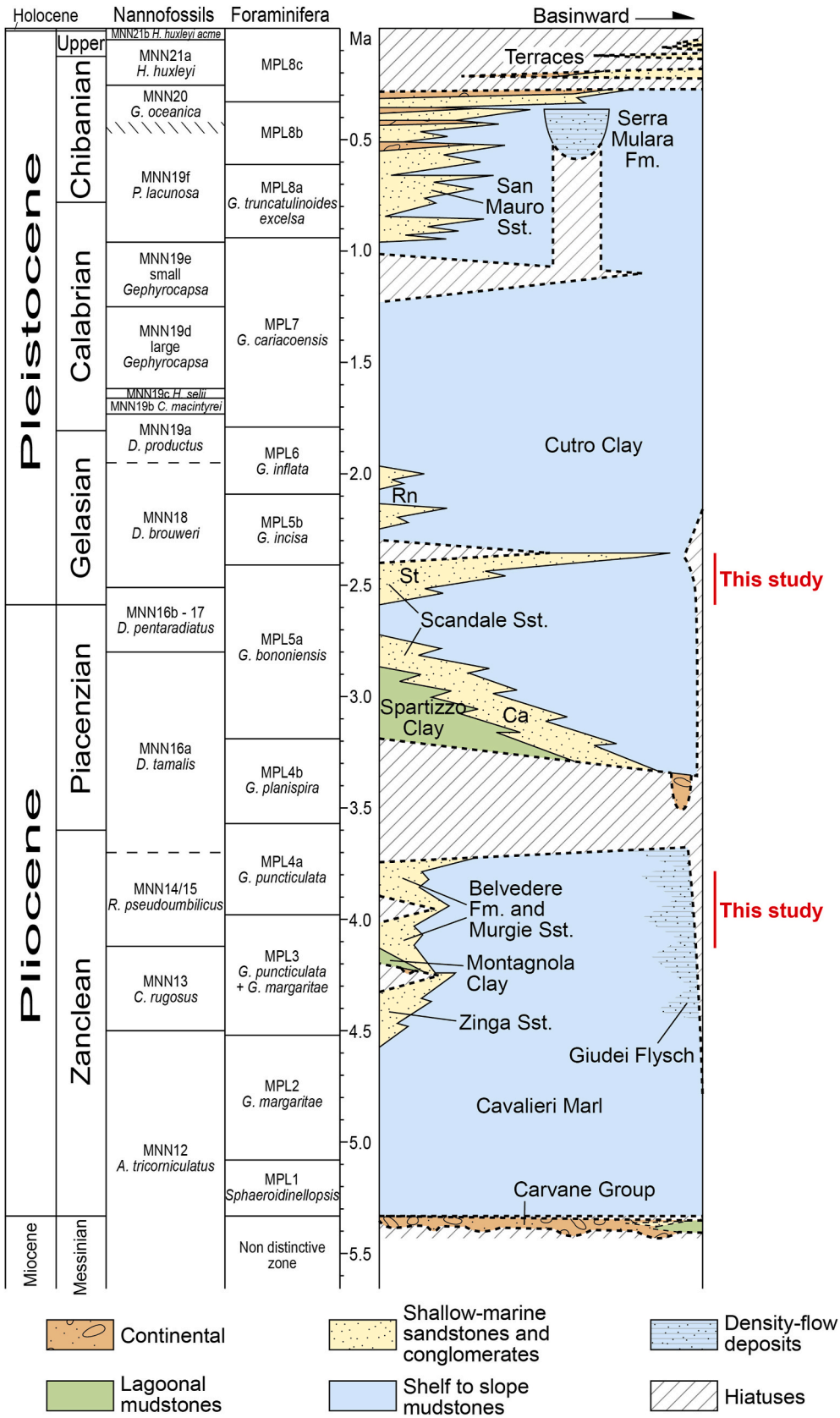

Fig. 2. The Plio-Pleistocene part of the sedimentary succession of the Crotone Basin (modified from Zecchin et al., 2020), compared with the IUGS International Chronostratigraphic Chart (https://stratigraphy.or g/ICSchart/ChronostratChart2021-05.pdf), and the calcareous nannofossil and planktonic foraminifera biostratigraphic schemes by Cita (1975), Rio et al. (1990), Lourens et al. (1996) and Raffi et al. (2006). The studied succession is part of the Zanclean Belvedere Formation and the Gelasian Strongoli Member of the Scandale Sandstone. Abbreviations: Ca – Casabona Member; Rn – Rocca di Neto Member; St – Strongoli Member.

Table 1
Facies and depositional environments of the studied deposits.

Facies association and facies	Lithology and thickness	Sedimentary structures and bioturbation	Fossils	Interpretation
A – Condensed shallow-marine				
A1: Wave-dominated shell-rich deposit	Stacked shell beds forming tabular cemented units 0.3–1° m thick. The grain size of the matrix ranges from fine-grained siliciclastic sandstone to granule-grade conglomerate and contains shell debris of variable amount. Cobbles and pebbles of sandstone may be found at the base.	Planar stratification and local swaley cross-stratification. Structureless in places. Local upward decreasing shell abundance. Occasional channel-like features down to 0.3° m at the base. Common substrate-controlled *Glossifungites* Ichnofacies at the base. Scattered bioturbation in the body. Erosional base and sharp to gradual upward transition into Facies B2.	Ostreids, pectinids and minor venerids (usually disarticulated and broken), usually convex-up arranged (also concave-up and edgewise arranged). Barnacles are common locally. Shells form stacked horizontal sheets or can be chaotically packed.	Shoreface deposit recording low net sedimentation rates, high-energy wave action and high - (Norris, 1986; Kidwell, 1991; Zecchin et al., 2017; 2019, 2021, 2022).
A2: Current-dominated shell-rich deposit	Very coarse-grained siliciclastic sandstone to pebbly conglomerate with shells, up to 1.5° m thick.	Unidirectional cross-stratified sets 0.2–1° m thick. Erosional base and sharp to gradual transition into Facies A1 or B2. A conglomerate lag 0.2° m thick can locally be present at the base.	Disarticulated and commonly broken ostreids and pectinids, with minor barnacles. Shells are aligned along the foresets, which in places show alternating shell-rich and siliciclastic components.	Large subaqueous dunes with probable tidal influence (Zecchin, 2005).
A3: Surface-related shell bed	Shell-rich fine-grained siliciclastic sandstone, 1 shell to 0.4° m thick.	Diffuse bioturbation and shell layers in the thicker beds, common substrate-controlled *Glossifungites* Ichnofacies up to 0.5° m deep at the base. Sharp base and top.	Disarticulated and locally broken pectinids, ostreids and minor venerids and barnacles, aligned on the basal surface or in layers within the thicker beds. Local presence of *Pinna nobilis* in life position at the base.	Community shell concentration recording low energy levels and sediment starvation in the distal lower shoreface (Kidwell et al., 1986; Norris, 1986; Cantalamessa et al., 2005; Zecchin et al., 2021).
B – Siliciclastic shoreface				
B1: Sand and mud	Very fine-grained quartz sandstone with silt matrix 3–-4° m thick	Structureless, rare cm-scale sand layers, sparse bioturbation. Gradational upper boundary with Facies B2.	Venerids, pectinids and gastropods	Shoreface-shelf transition (Galloway and Hobday, 1996; Clifton, 2006; Zecchin et al., 2022).
B2: Burrowed sandstone	Fine- to medium-grained siliciclastic sandstone 0.7–7.5° m thick.	Mostly structureless to planar stratified, scattered bioturbation, locally intense. The boundaries are sharp to gradual with Facies A1-A3, B1 and B3.	Sparse disarticulated (whole in places) pectinid, ostreid and venerid shells. Barnacles are also common. Gastropods, echinids, and disarticulated cardids and *Pinna nobilis* are locally present.	Lower shoreface (Galloway and Hobday, 1996; Reading and Collinson, 1996; Clifton, 2006; Zecchin et al., 2017; 2021, 2022).
B3: Hummucky and swaley cross-stratified to planar-laminated sandstone	Medium- to very coarse-grained siliciclastic sandstone and granule-grade conglomerate locally, up to 2° m thick.	Hummocky or swaley cross stratification to planar lamination. Scattered bioturbation. Gradual lower boundary with Facies B2 and erosional top, usually overlain by Facies A1.	Disarticulated and locally broken pectinid and ostreid shells, mainly convex-up arranged. Among the pectinids, *Amusium* sp. is locally very abundant and can form the whole association.	Storm-dominated lower to middle shoreface (Dott and Bourgeois, 1982; Dumas et al., 2005; Leckie and Walker, 1982; Zecchin et al., 2017; 2021).
B4: Planar stratified sandstone and conglomerate	Very coarse-grained siliciclastic sandstone to granule-grade conglomerate.	Planar stratification (dm-scale beds). Rare bioturbation. The lower boundaries are not visible. Erosional upper boundary with Facies A2.	Disarticulated and locally broken ostreid shells.	Storm-dominated upper shoreface (Massari and Parea, 1988; Hart and Plint, 1995; Clifton, 2006).

main forcing mechanisms, which are most likely related to the Milankovitch orbital cyclicity, are discussed herein. The results allow improving the knowledge on the impact of orbital forcing on the architecture of shallow-marine high-frequency sequences, and on the variations of this control during the Neogene and Quaternary.

2. Geological setting

The Neogene to Quaternary Crotone Basin lies on the Ionian side of the Calabrian Arc, a composite terrane made up of metamorphic, plutonic and sedimentary units and located between the NW-trending southern Apennines and the E-trending Sicilian Maghrebides (Amodio Morelli et al., 1976; Van Dijk et al., 2000; Bonardi et al., 2001) (Fig. 1A). The evolution of the Calabrian Arc was characterized by a SE-ward migration since Middle Miocene, which was paralleled by the subduction of the Ionian oceanic crust and the opening of the Tyrrhenian backarc basin (Malinverno and Ryan, 1986; Faccenna et al., 2001, 2005; Sartori, 2003; Guillaume et al., 2010; Critelli, 2018; Tripodi et al., 2018; Critelli and Martín-Martín, 2022, 2024) (Fig. 1A).

The evolution of the Crotone Basin (Fig. 1B), interpreted as a forearc depocenter active since the late Serravallian, was characterized by alternating phases of tectonic subsidence and uplift plus basin closure (Roda, 1964; Van Dijk, 1990; Zecchin et al., 2006, 2012, 2020; Massari and Prosser, 2013; Criniti et al., 2023). The sedimentary succession of the basin is heterogeneous and consists of Serravallian to Middle Pleistocene marine, coastal and continental deposits, recording both tectonic events and glacio-eustasy (Roda, 1964; Zecchin et al., 2004, 2012, 2013a, 2013b, 2015, 2020; Massari and Prosser, 2013).

The sedimentary succession considered in this study consists of two shallow-marine sandstone units, the Zanclean Belvedere Formation and the Gelasian Strongoli Member of the Scandale Sandstone (Fig. 2), which exhibit a spectacular meter-to decameter-scale high-frequency cyclicity (Zecchin, 2005; Zecchin et al., 2017, 2021, 2022). The main characteristics of these two units are described in Section 4.

3. Methods

The studied succession is described by seven measured sections (Fig. 1C,D and 3–13). A detailed facies analysis is the basis for the recognition of facies associations and depositional environments (Table 1), whereas depositional trends and key bounding surfaces are essential to define the sequence stratigraphic framework of the recognized stratigraphic sequences.

Ninety-nine sediment samples were collected along the measured

Fig. 3. (A) Typical appearance of the Belvedere Formation at the ZNE 2 section (Fig. 1D for location), with the boundaries of the upper high-frequency sequence highlighted in red. (B) Detail of the upper high-frequency sequence of the ZNE 2 section, bounded by wave-ravinement surfaces (WRS) and with a local flooding surface (LFS) in the middle. Facies code is in Table 1.

sections (Figs. 3–8 and 10–13), and approximately 100 g of sediment was taken from each sample for micropalaeontological analyses. The sample aliquots were dried at 50 °C for 24 h and then treated with hydrogen peroxide (10% vol) for 12 h, in order to remove the organic matter. Samples were then washed through a 125 μm mesh and dried. From the corresponding washing residues, 3 g of sediment was separated. All benthic foraminifera present in this amount of sediment were counted and classified following the taxonomic order of Loeblich and Tappan (1987).

4. The studied succession

4.1. Belvedere Formation

The Zanclean Belvedere Formation overlies deep-to shallow-water and paralic deposits and is truncated at the top by a regional unconformity, in turn overlain by transgressive Piacenzian deposits (Zecchin et al., 2012, 2020) (Fig. 2). The Formation, containing an intra-formational unconformity separating two higher rank sequences, consists of mixed siliciclastic and bioclastic shallow-marine deposits accumulated within half-graben sub-basins 2.5–5 km wide, and its thickness varies from few tens to some hundreds of meters due to syn-sedimentary normal faulting (Zecchin et al., 2004, 2006, 2012, 2017, 2020, 2021). The tectonically-controlled subsidence also led to a strong aggradational component of the Belvedere Formation (Zecchin et al., 2004, 2006). The alternation between shell-rich and siliciclastic sandstones defines a meter-to decameter-scale cyclicity (Fig. 3A and B), inferred to document Milankovitch-driven climatic changes leading to sediment supply changes and consequent alternating transgressive and normal regressive trends (Zecchin, 2005; Zecchin et al., 2017, 2021). Condensed, wave-dominated shell-rich transgressive deposits are locally replaced by shell-rich, meter-scale subaqueous dunes (Zecchin, 2005; Zecchin and Caffau, 2012). A typical cycle composing the Belvedere Formation is considered as a high-frequency sequence (Zecchin and Catuneanu, 2013; Catuneanu and Zecchin, 2013) bounded by ravinement surfaces, and consists of a transgressive systems tract (TST) made up of shell-rich deposits and in part of siliciclastic deposits, and of a highstand systems tract (HST) made up of siliciclastic deposits (Zecchin, 2005; Zecchin et al., 2017, 2021) (Fig. 3A and B).

Fig. 4. (A) Panoramic view of the Strongoli village (Fig. 1C for location), showing a gradual transition from the deep-water Cutro Clay to the shallow-water Strongoli Sandstone. (B) Detail of the Strongoli Sandstone with highlighted the Strongoli 2 and Strongoli 3 sections (Fig. 1C for location).

4.2. Strongoli Sandstone

The Gelasian Strongoli Member of the Scandale Sandstone, here simply referred to as the Strongoli Sandstone (Roda, 1964; Zecchin et al., 2022), is a progradational unit up to 70 m thick that pinches out basinward within the shelf to bathyal Cutro Clay (Capraro et al., 2006; Zecchin et al., 2012, 2020, 2022) (Figs. 2 and 4A). Overall, the unit shows a progressive shallowing-upward trend from shoreface-shelf transition to upper shoreface deposits (Zecchin et al., 2022). The lower transition between the Cutro Clay and the Strongoli Sandstone (Fig. 4A) consists of an alternation between silt and sand intervals (Zecchin et al., 2022). The uppermost part of the Formation documents increasing subsidence rates and rapid deepening to bathyal depths (Capraro et al., 2006; Zecchin et al., 2012, 2020, 2022). Following Capraro et al. (2006), the accumulation of the Strongoli Sandstone started around 2.6 Ma.

A high-frequency cyclicity in the Strongoli Sandstone has been recognized for the first time by Zecchin et al. (2022) and is described here in more detail. These cycles, consisting of high-frequency sequences bounded by wave-ravinement surfaces, exhibit transgressive and regressive intervals and are up to 7 m thick. The overall architecture of these high-frequency sequences resembles that of the high-frequency sequences composing the Belvedere Formation.

4.3. Facies and depositional environments

Being accumulated in similar shallow-marine settings, facies and depositional environments of the Belvedere Formation and Strongoli Sandstone are described together in Table 1. Seven marine facies are grouped into two facies associations (A – Condensed shallow-marine and B – Siliciclastic shoreface). Facies analysis of the Belvedere formation was extensively documented by Zecchin (2005) and Zecchin et al. (2017, 2021). Part of the Strongoli Sandstone was illustrated by Zecchin et al. (2022).

Facies association A usually contains shell-rich deposits inferred to have accumulated under conditions of net siliciclastic sediment bypass and/or starvation (Zecchin et al., 2017, 2021). Wave-dominated tabular shell-rich deposits (Facies A1) up to 1 m thick are by far the most common among those of facies association A, both in the Belvedere Formation and in the Strongoli Sandstone (Figs. 5–13 and 14A). They are rich of intra-basinal skeletal material, although relatively coarse-grained sediment reworked from the substrate can be present in varying proportions. On average, shells in Facies A1 are more abundant and densely packed in the Belvedere Formation than in the Strongoli

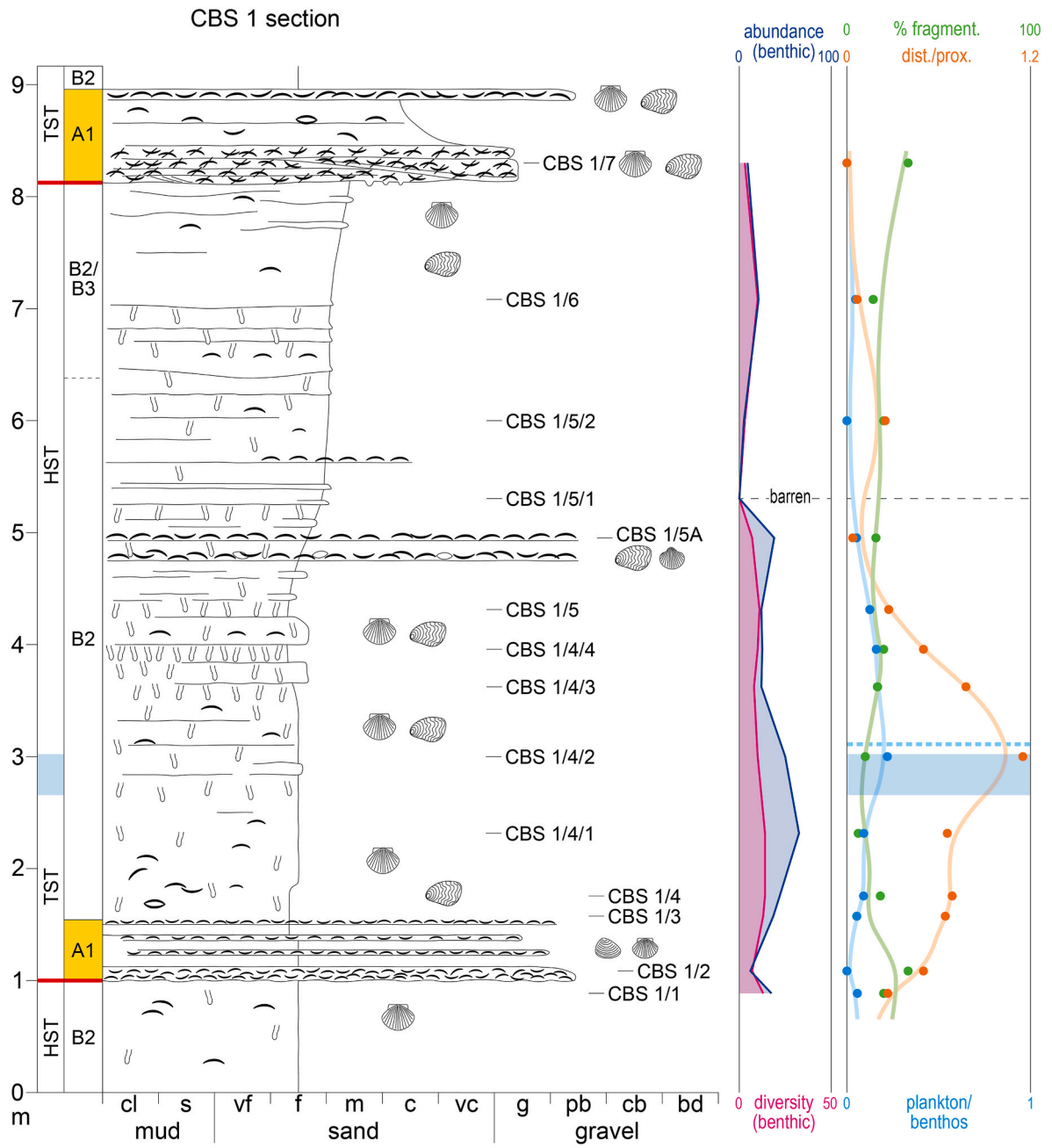

Fig. 5. The South Casabona (CBS) 1 section of the Belvedere Formation (Fig. 1D for location and Fig. 9 for symbols; modified from Zecchin et al., 2021). Sedimentary structures, fossils, samples, facies and facies contacts, sequence stratigraphic surfaces and systems tracts are shown on the left. The curves derived from the micropaleontological analysis (abundance, diversity, % fragmentation, distal/proximal and plankton/benthos, see text) are shown on the right.

Sandstone (Figs. 5–13). In some instances, Facies A1 in the Strongoli Sandstone shows intermediate features with Facies B2 (Fig. 11). A substrate-controlled *Glossifungites* Ichnofacies at its erosional base is a common characteristic of Facies A1 (Figs. 3B and 7-13), which is inferred to have accumulated under high-energy conditions due to the repeating action of waves and storm flows, low net deposition due to sediment bypass during coastal retreat, and climatic and trophic conditions favoring the development of mollusk communities (Norris, 1986; Kidwell, 1991; Fürsich and Oschmann, 1993; Meldahl, 1993; Naish and Kamp, 1997a; Kondo et al., 1998; Fürsich and Pandey, 1999; Cantalamessa et al., 2005; Zecchin et al., 2017, 2021). Facies A2 is found only in the Belvedere Formation and is considered as an equivalent of Facies A1 under depositional conditions dominated by relatively strong currents that favored the migration of large dunes, which in the considered measured sections are up to 1 m thick (Figs. 6–8 and 14B). The local evidence of alternating shell-rich and siliciclastic foresets (Fig. 6) suggests the action of tidal currents (e.g., Longhitano et al., 2012), which were enhanced due to lateral confinement within the half-graben sub-basins in which the Belvedere Formation accumulated (Zecchin, 2005). Facies A3 is commonly associated with bioturbation, locally well-developed *Glossifungites* Ichnofacies at its base and in places by shells in life position, documenting sediment starvation and lower energy levels in relatively distal settings (Kidwell et al., 1986; Norris, 1986; Meldahl, 1993; Cantalamessa et al., 2005; Zecchin et al., 2021) (Figs. 7, 8, 10, 11 and 14C). In the Strongoli Sandstone, the basal surface associated with substrate-controlled ichnofacies was locally observed with no or extremely thin deposits of Facies A3 (Figs. 10–12).

Facies association B is characterized by siliciclastic deposits

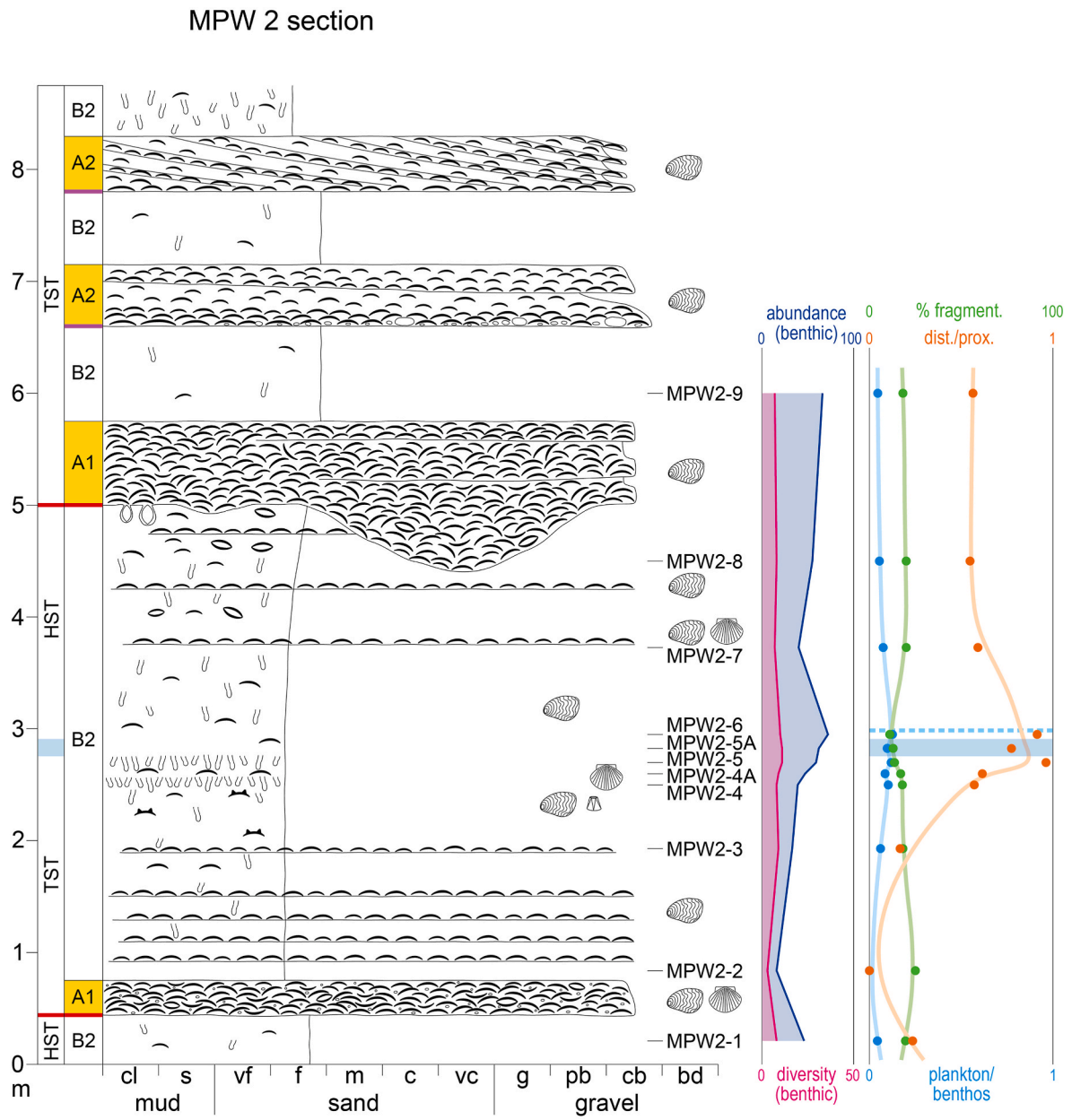

Fig. 6. The West Montagna Piana (MPW) 2 section of the Belvedere Formation (Fig. 1D for location and Fig. 9 for symbols). Sedimentary structures, fossils, samples, facies and facies contacts, sequence stratigraphic surfaces and systems tracts are shown on the left. The curves derived from the micropaleontological analysis (abundance, diversity, % fragmentation, distal/proximal and plankton/benthos, see text) are shown on the right.

accumulated from shoreface-shelf transition to upper shoreface depositional settings. Shoreface-shelf transition deposits are represented by very fine-grained sandstones with mud matrix (Facies B1) in the lowermost part of the Strongoli Sandstone (Zecchin et al., 2022, Fig. 9). Facies B2, consisting of burrowed sandstone with sparse bivalve shells and shell layers, is the most common facies in both the Belvedere Formation and the Strongoli Sandstone (Figs. 5–13 and 14A,B,C) and is inferred to have accumulated in lower shoreface settings (Table 1). This facies commonly alternates with the deposits of the facies association A (Figs. 6–8, 10, 11 and 14C), and may overlie Facies B1 and/or grade upward into Facies B3 via an interval of intermediate characteristics between those of Facies B2 and B3 (Figs. 5, 9 and 12). Facies B3 shows packed shell beds and common hummocky or swaley cross-stratification (Figs. 12, 13 and 14D), indicating repeating storm events and higher energy level in lower to middle shoreface depositional settings. Upper shoreface deposits are represented by the planar-stratified Facies B4, which in the selected sections are found only in the Belvedere Formation and are among the coarsest sediments in the studied succession (Fig. 7). Due to their scarceness, deposits of Facies B4 are never seen to overlie Facies B2 and B3 (Figs. 5–13). Trough cross-stratified upper shoreface deposits are abundant in some intervals of the Belvedere Formation and occasionally in the uppermost part of the Strongoli Sandstone (Zecchin et al., 2021).

5. Micropaleontological analysis

Given the proximal depositional settings characterizing the studied succession, the analysis of 3 g of sediment of the collected samples documents an abundance of reworked specimens, not considered for the analysis, as well as intra-basinal specimens dominated by very shallow-water benthic foraminifera species, consisting of *Ammonia* spp. and *Elphidium* spp. (Abbott, 1997; Naish and Kamp, 1997b; Donnici and

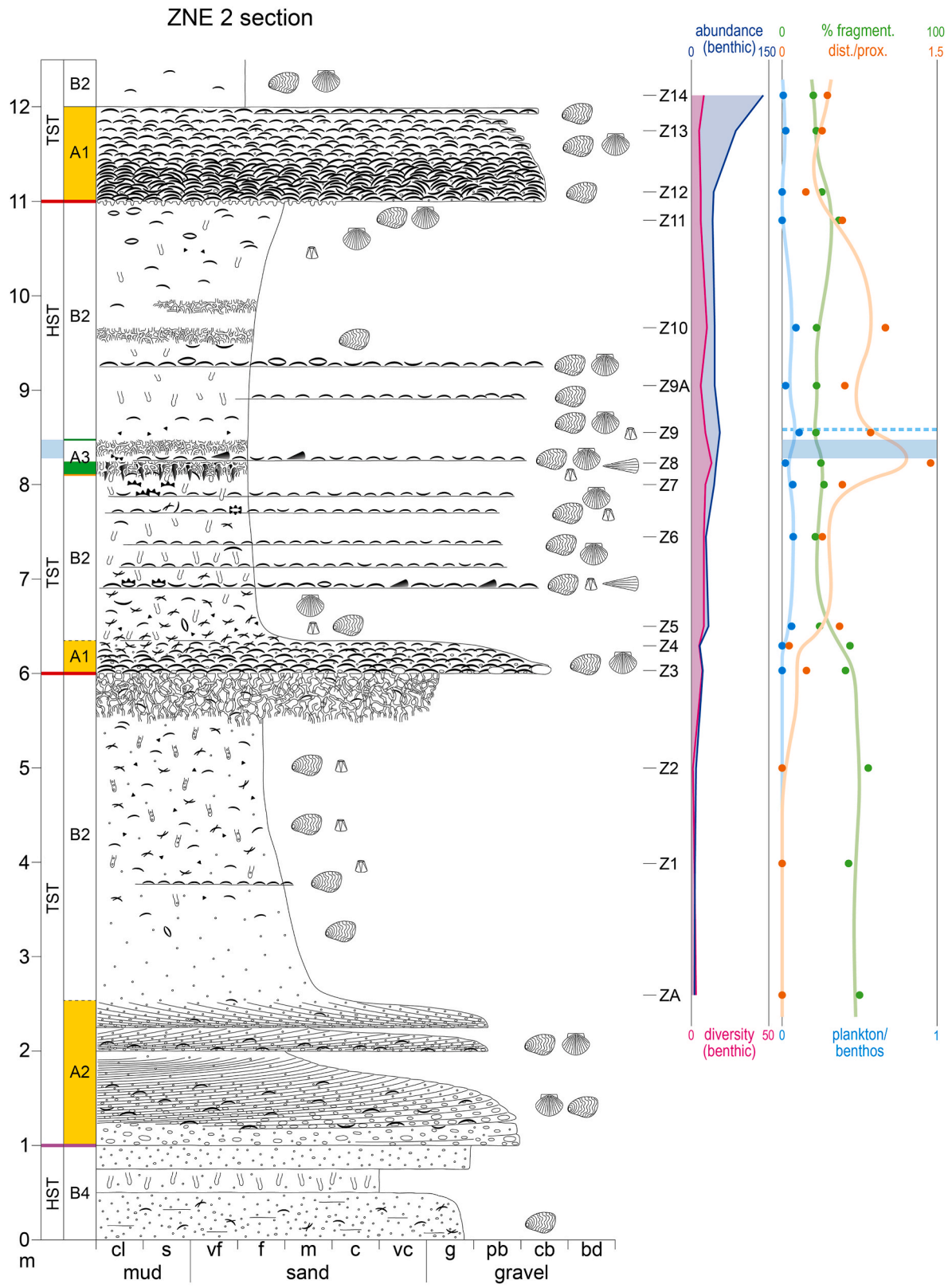

Fig. 7. The East Zinga (ZNE) 2 section of the Belvedere Formation (Fig. 1D for location and Fig. 9 for symbols; modified from Zecchin et al., 2021). Sedimentary structures, fossils, samples, facies and facies contacts, sequence stratigraphic surfaces and systems tracts are shown on the left. The curves derived from the micropaleontological analysis (abundance, diversity, % fragmentation, distal/proximal and plankton/benthos, see text) are shown on the right.

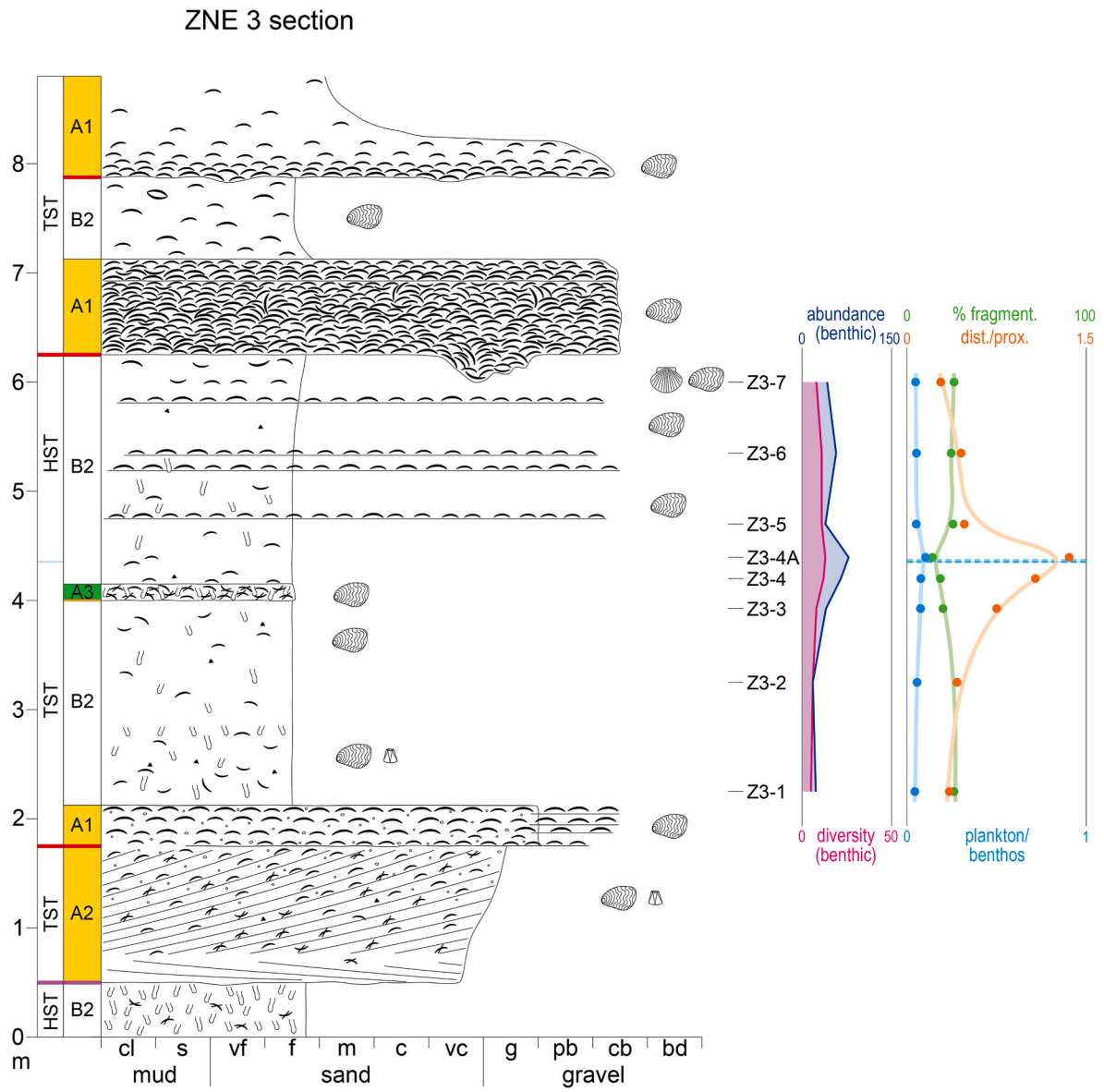

Fig. 8. The East Zinga (ZNE) 3 section of the Belvedere Formation (Fig. 1D for location and Fig. 9 for symbols). Sedimentary structures, fossils, samples, facies and facies contacts, sequence stratigraphic surfaces and systems tracts are shown on the left. The curves derived from the micropaleontological analysis (abundance, diversity, % fragmentation, distal/proximal and plankton/benthos, see text) are shown on the right.

Serandrei-Barbero, 2002; Mendes et al., 2004) (see Supplementary data). Where the depositional settings are less proximal, the abundance of relatively distal species, such as *Amphycorina scalaris*, *Bolivina* spp., *Bulimina* spp., *Globobulimina affinis*, *Cibicidoides pseudoungerianus*, *Nonion fabum*, *Florilus boueanum*, and *Uvigerina* spp., increases (e.g., Stefanelli, 2003; Morigi et al., 2005; Phipps et al., 2010) (Supplementary data). Intra-basinal planktonic foraminifera are relatively scarce and always transported in the studied deposits. They are mainly represented by *Globigerina bulloides* and *Globigerinoides ruber*.

The micropaleontological analysis was used in this study to define three parameters, which were successfully applied by Zecchin et al. (2021, 2022) for the sequence stratigraphic analysis of Plio-Quaternary successions in the Crotone Basin. These parameters consist of the '% fragmentation' (Fr; the percentage of fragmentation of intra-basinal benthic foraminifera for each sample), the 'distal/proximal' (D/P; the ratio between relatively distal and proximal species of benthic foraminifera for each sample), and the 'plankton/benthos' (P/B; the ratio between the number of planktonic foraminifera and benthic foraminifera for each sample) (Figs. 5–8 and 10-13). According to Zecchin et al. (2021, 2022, 2023), the Fr parameter is considered as a proxy for energy (effectiveness of waves and currents), in turn linked to changes of local energy or shoreline shift, whereas the D/P parameter is expected to reflect variations of sedimentation rates linked to shoreline shifts and therefore it is useful to recognize transgressive and regressive trends. Maximum values of the D/P parameter, concomitant with minimum values of the Fr parameter (Figs. 5–8 and 10-13), should reflect maximum flooding conditions. In contrast with the D/P parameter, the P/B parameter is inferred to reflect the water mass rather than the substrate, and therefore it is expected to reflect water depth changes, with higher values indicating deeper conditions (Zecchin et al., 2021, 2022, 2023).

According with Zecchin et al. (2021, 2022), for the D/P parameter the following formula has been considered:

D/P = (% *Amphycorina scalaris* + % *Bolivina* spp. + % *Bulimina* spp. + % *Globobulimina affinis* + % *Cibicidoides pseudoungerianus* + % *Nonion fabum* + % *Florilus boueanum* + % *Uvigerina* spp.)/(% *Ammonia* spp. + % *Elphidium* spp.)

For more information on the advantages of employing these

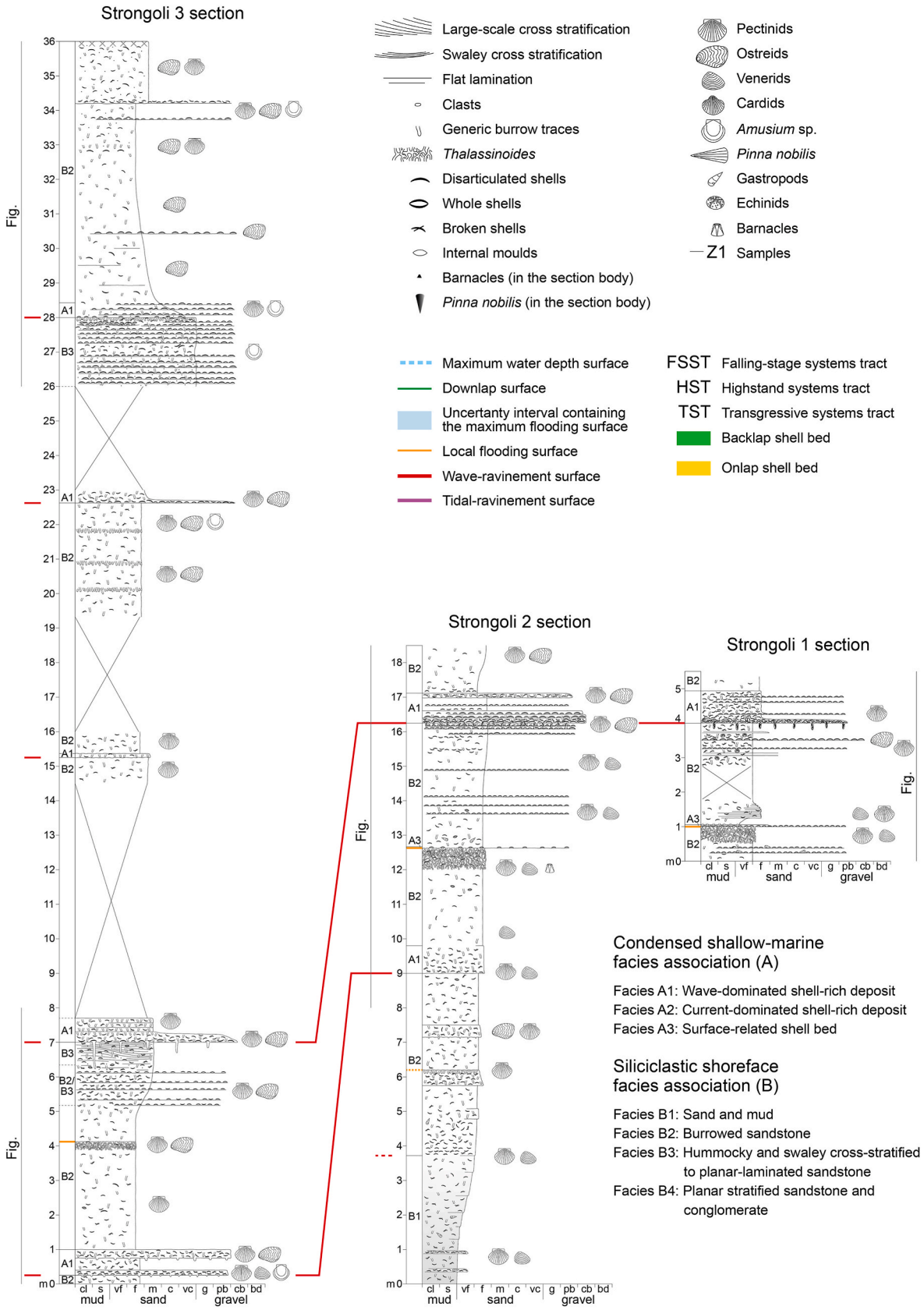

Fig. 9. The measured sections documenting the Strongoli Sandstone (Strongoli 1, 2 and 3; Fig. 1C for location). Details of the sections are shown in Figs. 10–13. Symbols for all sections of this study are also reported.

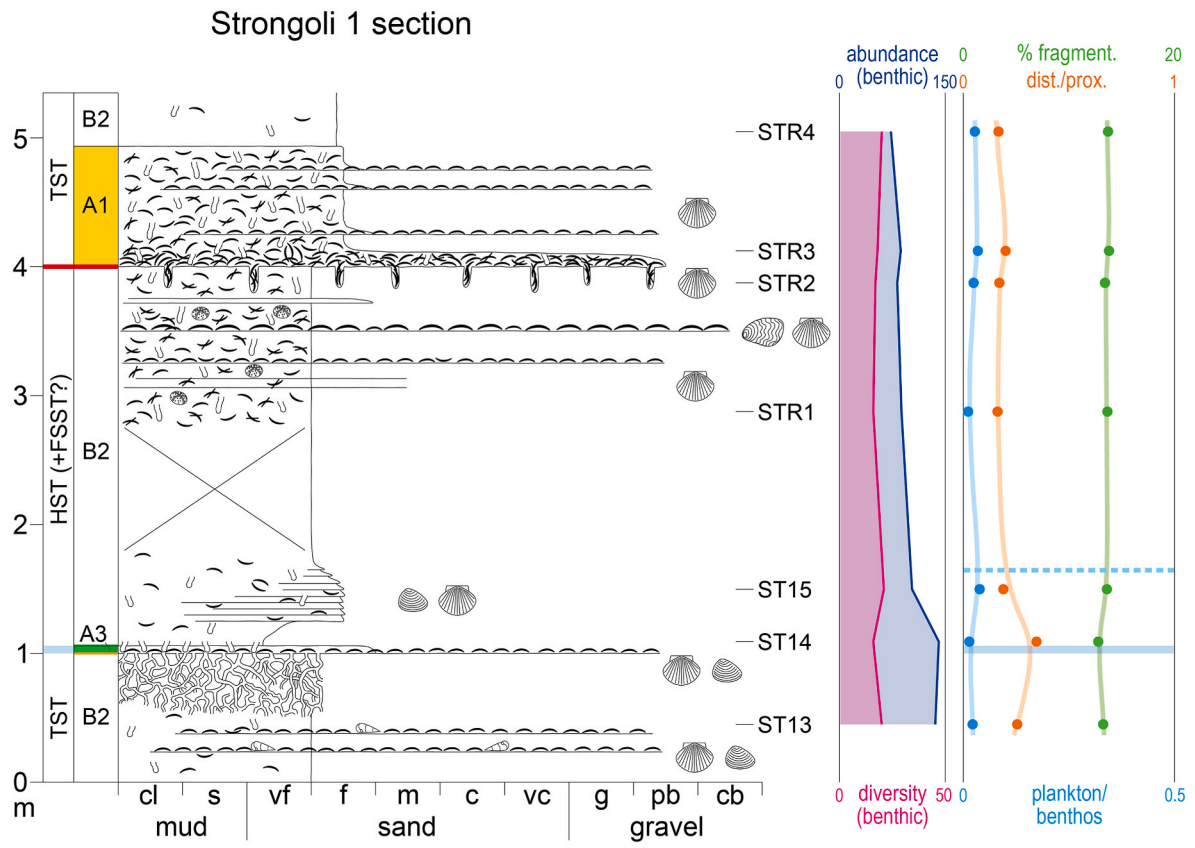

Fig. 10. The Strongoli 1 section of the Strongoli Sandstone (Fig. 1C for location and Fig. 9 for symbols). Sedimentary structures, fossils, samples, facies and facies contacts, sequence stratigraphic surfaces and systems tracts are shown on the left. The curves derived from the micropaleontological analysis (abundance, diversity, % fragmentation, distal/proximal and plankton/benthos, see text) are shown on the right.

parameters over others already used for sequence stratigraphic studies, such as the abundance and diversity of benthic foraminifera (e.g., Fillon, 2007; Gutiérrez Paredes et al., 2017), see Zecchin et al. (2021, 2022, 2023).

6. Stratigraphic architecture

6.1. *High-frequency sequences of the Belvedere Formation*

According to Zecchin et al. (2017, 2021), the erosional base of the facies association A, commonly typified by substrate-controlled *Glossifungites* Ichnofacies and overlain by condensed shell beds (Facies A1), is interpreted as a wave-ravinement surface (WRS; Zecchin et al., 2019) (Fig. 3B, 5-8 and 14A). Where the surface is overlain by large subaqueous dunes (Facies A2), inferred to be controlled by tidal currents, it is interpreted as tidal-ravinement surface (TRS; Allen and Posamentier, 1993) (Figs. 6–8 and 14B). WRSs and TRSs can locally be present together in the same sequence (Fig. 6). Given their position directly above the RS, the shell-rich Facies A1 and A2 are considered as onlap shell beds (OSB; Kidwell, 1991; Naish and Kamp, 1997a; Kondo et al., 1998) (Figs. 5–8), documenting repeating storm reworking of shells and sediment bypass during transgression. However, the shell abundance in Facies A1 and A2 may at least in part be related to climatic conditions favoring shell production (Zecchin et al., 2017). Being the most prominent surface in the studied succession, the wave- or tidal-RSs are the best choice as boundaries of high-frequency sequences (e.g., Zecchin et al., 2017, 2021, 2022).

A number of 30–35 high-frequency sequences has been estimated in the Belvedere Formation; they are usually composed of deposits of Facies A1 and/or A2 at the base, overlain by deposits of Facies B2, and are 4.5–7 m thick in the considered sections (Figs. 5–8). Facies B2 can be interrupted by Facies A3 in a roughly mid-sequence position, and can grade upwards into Facies B2/B3 transitional deposits (Figs. 5, 7, 8 and 14C). Facies A1 and A2 can be separated by facies B2 intervals (Fig. 6), and this situation probably reflects a punctuated transgression, characterized by two or more transgressive pulses separated by pauses in coastal retreat (Swift et al., 1991; Zecchin et al., 2019, 2021). Facies B4 is found in the lower part of the Belvedere Formation, where the succession is dominated by relatively coarse-grained deposits and the high-frequency cyclicity is difficult to recognize (Fig. 7). Trough cross-bedded, upper shoreface sandstones are common only in high-frequency sequences in the upper part of the two higher rank sequences of the Belvedere Formation (Zecchin et al., 2012, 2020, 2021) and are not considered in this study, as the recognition of lower rank maximum flooding surfaces (MFS) is more difficult in that cases (Zecchin et al., 2021). Given the scarce facies variability observed in the studied high-frequency sequences, the magnitude of transgressions and regressions is inferred to be very modest, as the depositional system always remains within the shoreface division.

Following Zecchin et al. (2021, 2022, 2023), the best indicator of the position of the MFS, separating transgressive and normal regressive deposits, is represented by an uncertainty interval between the negative peak of the Fr parameter and the positive peak of the D/P parameter, which are always close; this interval varies between few cm to ca. 0.35 m in the considered sequences, and excepting the CBS 1 section, it typically falls in a roughly mid-sequence position (Figs. 5–8). The uncertainty interval indicates that the MFS is usually cryptic and that in general it cannot be pinpointed based on direct field evidence alone, being placed within a sand interval that does not exhibit diagnostic features such as lithological variability (Figs. 5–8).

The uncertainty interval containing the MFS is inferred to separate the transgressive systems tract (TST) of the high-frequency sequences,

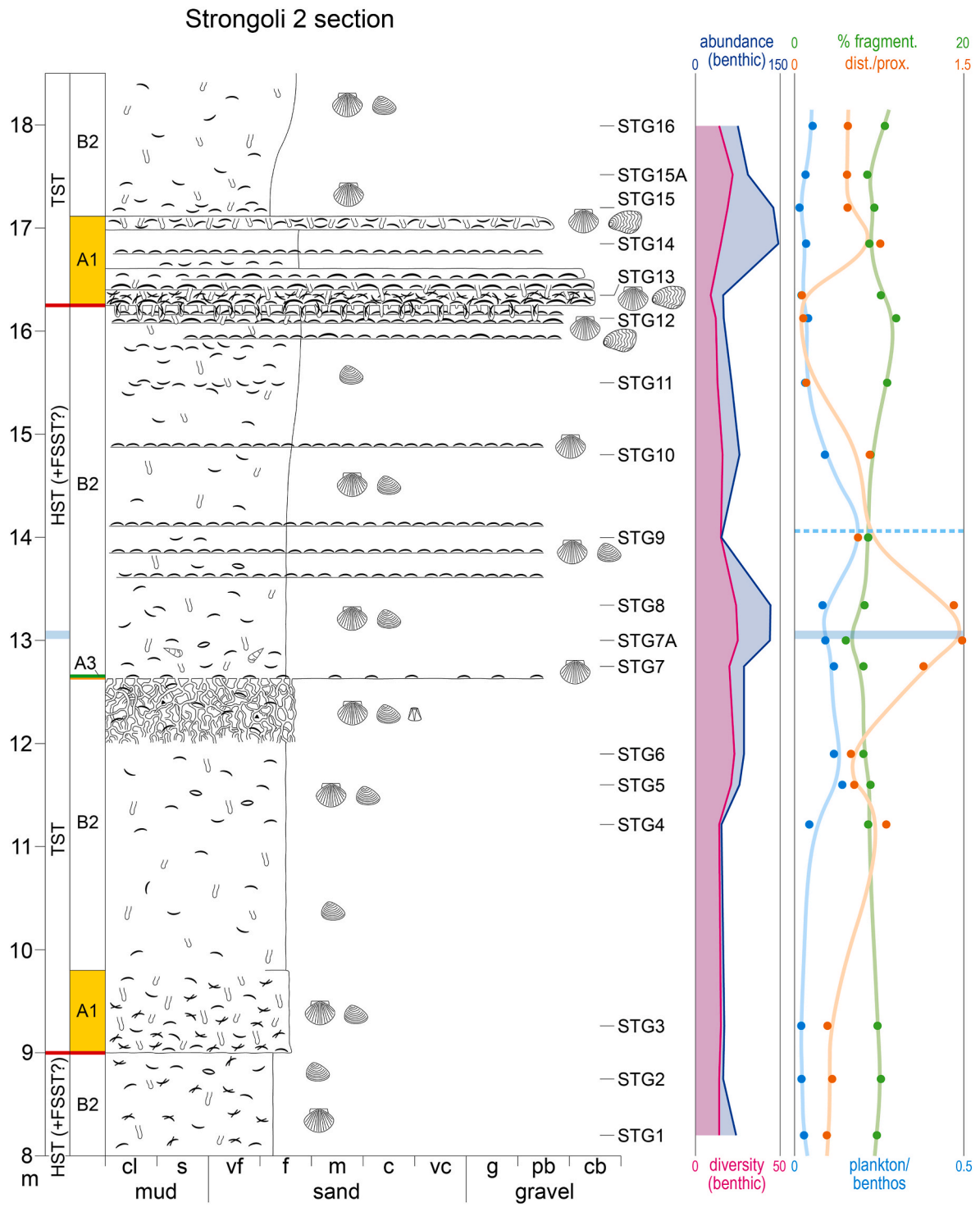

Fig. 11. The Strongoli 2 section of the Strongoli Sandstone (Fig. 1C for location and Fig. 9 for symbols; modified from Zecchin et al., 2022). Sedimentary structures, fossils, samples, facies and facies contacts, sequence stratigraphic surfaces and systems tracts are shown on the left. The curves derived from the micropaleontological analysis (abundance, diversity, % fragmentation, distal/proximal and plankton/benthos, see text) are shown on the right.

composed of deposits of Facies A1/A2 at the base, overlain by deposits of Facies B2, from the highstand systems tract (HST), dominated by deposits of Facies B2 (Figs. 5–8 and 15A). As stated above, the limited facies change in the upper part of the high-frequency sequences, consisting of only a slight upward increase in grain size and frequency of individual shell beds in Facies B2 (Figs. 6–8), or of a transition toward Facies B3 (Fig. 5), points to a very modest normal regressive trend, whereas forced regressive deposits, usually featured by a strong progradational component, are probably absent (Fig. 15A).

The base of Facies A3, which is located in a roughly mid-sequence position, always below the base of the uncertainty interval containing the MFS and locally associated with substrate-controlled *Glossifungites* Ichnofacies (Fig. 3B, 7 and 8 and 14C), probably reflects conditions of sediment starvation in relatively distal settings near the end of the transgression; it can be considered as a local flooding surface (LFS), as defined by Abbott and Carter (1994) (see also Zecchin and Catuneanu,

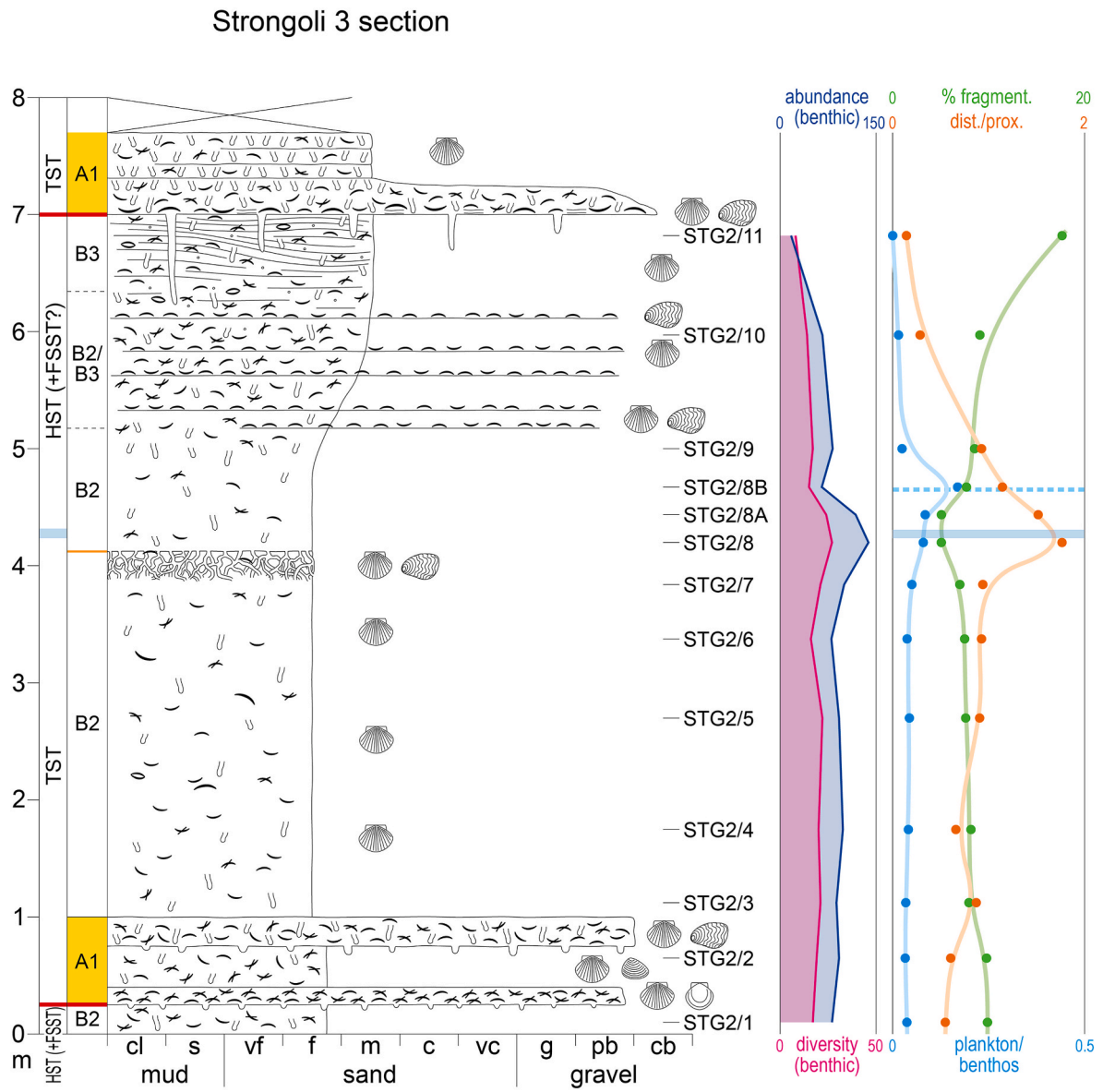

Fig. 12. The lower part of the Strongoli 3 section of the Strongoli Sandstone (Fig. 1C for location and Fig. 9 for symbols). Sedimentary structures, fossils, samples, facies and facies contacts, sequence stratigraphic surfaces and systems tracts are shown on the left. The curves derived from the micropaleontological analysis (abundance, diversity, % fragmentation, distal/proximal and plankton/benthos, see text) are shown on the right.

2013; Zecchin et al., 2021). The overlying shell bed of Facies A3, therefore, can be considered as a backlap shell bed (BSB; Kidwell, 1991; Naish and Kamp, 1997a; Kondo et al., 1998; Di Celma et al., 2005) (Figs. 7 and 8), developing near the end of transgressive phases and documenting sediment starvation and relatively lower energy levels, as testified by the local presence of shells in life position (Figs. 7 and 14C). The development of BSBs is variable, and they represent part or the whole condensed section of stratigraphic sequences (Zecchin and Catuneanu, 2013, 2023). Unlike Zecchin et al. (2021), in this study the uncertainty interval in the ZNE 2 section is not equated to the whole condensed section represented by Facies A3, but it is defined between the positive peak of the D/P parameter below and the downlap surface (DLS) above (Fig. 7). The DLS (Figs. 7 and 14C) is a facies contact between the condensed section and the overlying prograding clastic wedge, and tends to disappear landwards (Zecchin and Catuneanu, 2013 and references therein; Zecchin et al., 2023). If the top of Facies A3 is below the uncertainty interval containing the MFS, that facies contact is assumed not to correspond to the DLS (Fig. 8), which should be placed above of, or at most coincident with, the MFS (Fig. 7).

The maximum water depth within stratigraphic sequences is thought to be associated with the maximum abundance of planktonic foraminifera relative to benthic foraminifera, and this condition is inferred to be indicated by the maximum water depth surface (MWDS), a cryptic surface that coincides with the peak of the P/B curve (Zecchin et al., 2021, 2022, 2023) (Figs. 5–8). The MWDS is expected to lie in the lower HST, during initial normal regressive conditions, until the progradation of the clastic wedge triggers a bathymetric decrease (Abbott, 1997; Carter et al., 1998; Catuneanu, 2006; Zecchin et al., 2021, 2022). In fact, in the considered high-frequency sequences of the Belvedere Formation, the MWDS always lies above of, or coincides with, the upper boundary of the uncertainty interval containing the MFS, as expected (Figs. 5–8).

The high-frequency sequences of the Belvedere Formation, therefore, consist of T-R sequences (Johnson and Murphy, 1984; Embry and Johannessen, 1992) few meters thick, bounded by RSs and commonly showing a symmetric architecture with transgressive and normal regressive shoreface deposits of similar thickness (i.e., the T-R cycle architecture of Zecchin, 2007) (Figs. 6–8 and 15A). In some cases, the sequences are asymmetric, dominated by normal regressive deposits

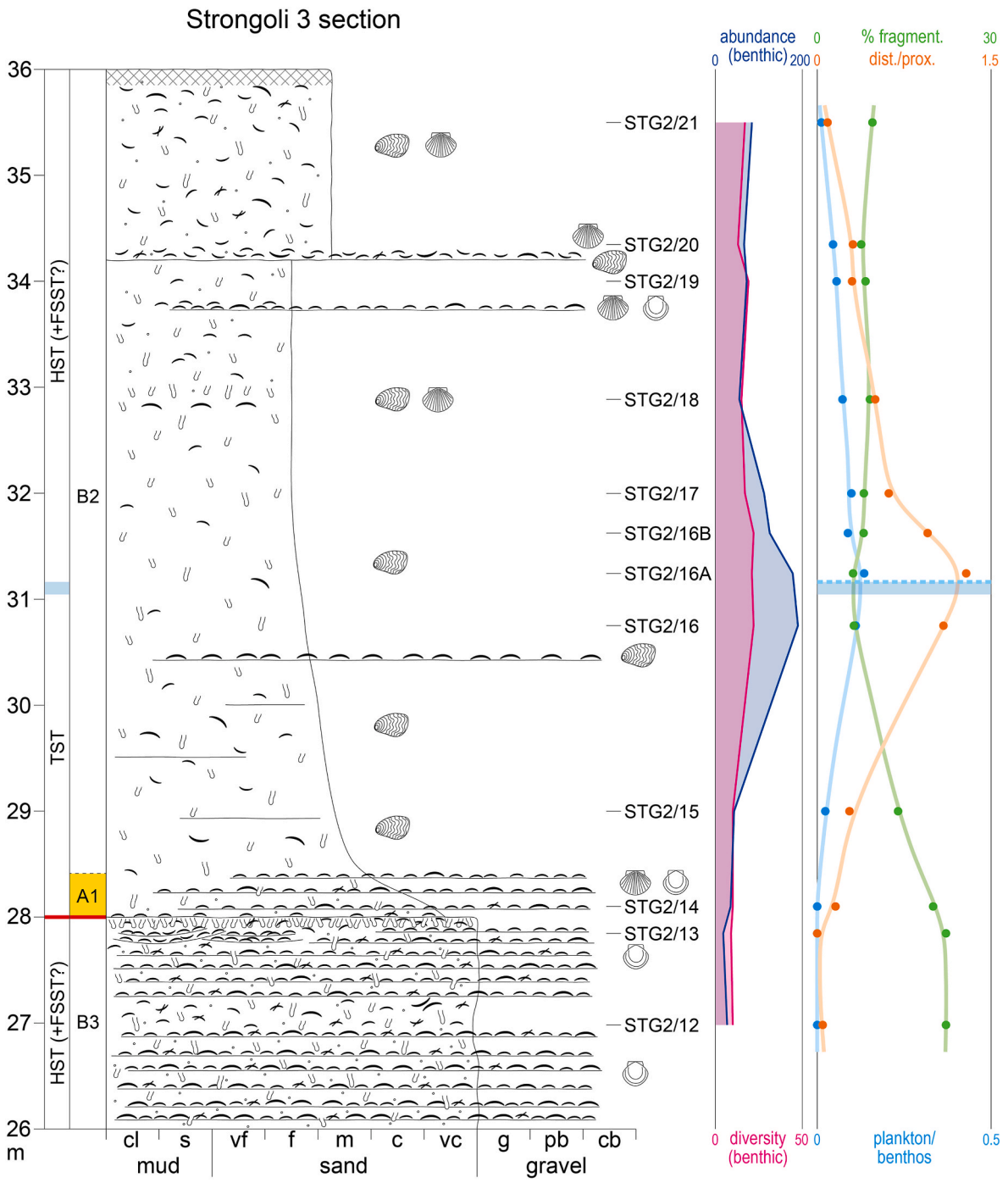

Fig. 13. The upper part of the Strongoli 3 section of the Strongoli Sandstone (Fig. 1C for location and Fig. 9 for symbols). Sedimentary structures, fossils, samples, facies and facies contacts, sequence stratigraphic surfaces and systems tracts are shown on the left. The curves derived from the micropaleontological analysis (abundance, diversity, % fragmentation, distal/proximal and plankton/benthos, see text) are shown on the right.

(the R cycle architecture of Zecchin, 2007), resembling the classic parasequence architecture (Van Wagoner et al., 1988, 1990) (Fig. 5). More rarely, in cases where large subaqueous dunes (Facies A2) are present in the lower part of the sequences, transgressive deposits are dominant or are the only ones preserved (the T Cycle architecture of Zecchin, 2007) (Figs. 7 and 8). The most peculiar case is that of the ZNE 2 section, where the lower sequence is significantly coarser-grained compared to the others and shows only an overall fining- and deepening-upward trend from Facies A2 to Facies B2 (Fig. 7). The regressive part of that sequence was likely removed by wave erosion during the following transgression.

The high-frequency sequence documented by the middle to upper part of the ZNE 2 section (Figs. 7 and 16) is one of the best preserved of the Belvedere Formation and is also documented in the middle part of the ZNE 3 section (Figs. 8 and 16). The sequence exhibits just a slight distal setting in the ZNE 2 section, compared to the ZNE 3 section (Fig. 16), as documented by finer-grained deposits with *Pinna* shells in life position characterizing Facies A3, which is topped by the DLS only in the former. Moreover, the ZNE 2 section, although relatively close to the ZNE 3 section, documents a succession sedimented in an area of overall higher subsidence rate, being closer to the fault margins of the half-graben sub-basins in which the Belvedere Formation accumulated. This difference in accommodation is highlighted by the variable

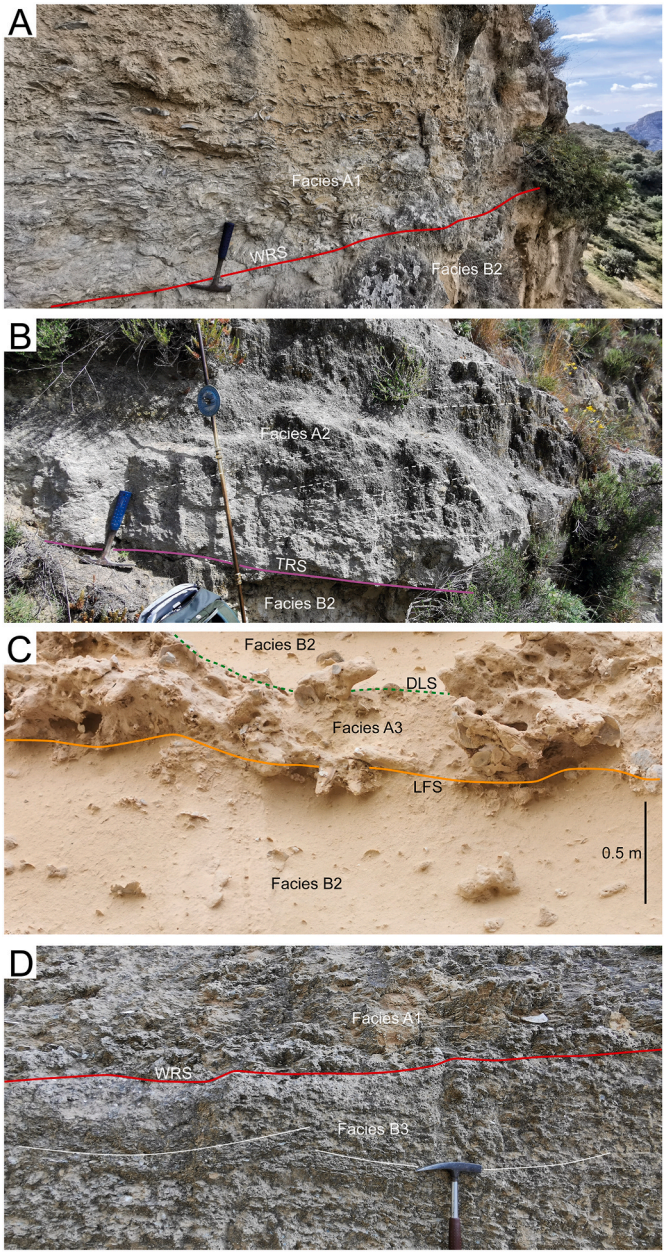

Fig. 14. Examples of facies in the studied deposits. (A) Erosional contact between burrowed sandstones (Facies B2) and wave-dominated shell-rich deposits (Facies A1) in the ZNE 2 section. (B) (A) Erosional contact between burrowed sandstones (Facies B2) and current-dominated shell-rich deposits (Facies A2) in the ZNE 3 section. (C) Burrowed, surface-related shell bed (Facies A3) within burrowed sandstones of Facies B2 (ZNE 2 section, modified from Zecchin et al., 2021). (D) Erosional contact between swaley cross-stratified to planar-laminated sandstones (Facies B3) and wave-dominated shell-rich deposits (Facies A1) in the Strongoli 3 section (modified from Zecchin et al., 2022). Abbreviations: DLS – downlap surface; LFS – local flooding surface; TRS – tidal-ravinement surface; WRS – wave-ravinement surface.

preservation of the underlying high-frequency sequence, which is bounded by a TRS at the base and by a WRS at the top and is markedly truncated by the WRS in the ZNE 3 section, compared to the ZNE 2 section (Fig. 16).

The high-frequency sequences of the Belvedere Formation may locally show an internal heterogeneity, consisting of dm-to m-scale bedsets bounded by erosional or non-depositional surfaces (Zecchin et al., 2017), which are beyond the purpose of this study.

6.2. *High-frequency sequences of the Strongoli Sandstone*

Similarly to the high-frequency sequences of the Belvedere Formation, also for those composing the Strongoli Sandstone the best bounding surface is that at the base of the shell bed of Facies A1 (the OSB), interpreted as a WRS (Figs. 9–13). Six high-frequency sequences, 5–8 m thick, were recognized in the Strongoli Sandstone (Fig. 9); they are composed of Facies A1 at the base, passing upward into Facies B2 that locally grades into Facies B3 (Figs. 9–13). Facies A2 is absent in the Strongoli Sandstone. Facies B2 can be truncated in a roughly mid-sequence position by a surface marked by well-developed *Glossifungites* Ichnofacies, which can be paved by very thin deposits of Facies A3 (Figs. 10–12).

The uncertainty interval containing the MFS, between the negative peak of the Fr parameter and the positive peak of the D/P parameter (see Section 6.1), has a thickness that ranges between ca. 0.1 and 0.2 m and is inferred to separate the TST and the HST of the high-frequency sequences (Figs. 10–13). The uncertainty interval usually falls in a roughly mid-sequence position (Figs. 11 and 12), and therefore the high-frequency sequences of the Strongoli Sandstone exhibit a T-R cycle architecture (Zecchin, 2007).

As the surface marked by *Glossifungites* Ichnofacies found in a mid-sequence position is always below, or coincident with, the base of the uncertainty interval containing the MFS, it is interpreted as a LFS (Figs. 10–12), as in the case of the high-frequency sequences of the Belvedere Formation. The thin Facies A3 that locally overlies the LFS is therefore interpreted as a BSB (Figs. 10 and 11).

The MWDS, whose position is indicated by the peak of the P/B parameter, usually lies above the uncertainty interval (up to 1 m above), although in one case it coincides with the top of the interval itself (Figs. 10–13). As a general trend, the MWDS and MFS surfaces converge towards the shoreline, and diverge in a distal (basinward) direction (Catuneanu, 2006, 2022, Fig. 15B).

The best preserved high-frequency sequence of the Strongoli Sandstone is intercepted by the Strongoli 1, 2 and 3 sections (Fig. 17), which document a progressive deepening from the Strongoli 3 to the Strongoli 1 sections, as shown by the transition from lower-middle shoreface to distal lower shoreface deposits in the upper part of the sequence and by the presence of the DLS above Facies A3 only in the Strongoli 1 section (Figs. 10 and 17). However, the main features of the sequence, including the stratigraphic architecture, the relative position of the MFS and MWDS, as well as the presence of well-developed *Glossifungites* Ichnofacies at the LFS and the bounding WRSs, are persisting and well recognizable in all sections (Figs. 10–12 and 17).

Overall, the high-frequency sequences of the Strongoli Sandstone are therefore similar to those of the Belvedere Formation, sharing similar thicknesses, modest facies changes mainly represented by lower shoreface deposits, and a T-R cycle architecture. However, the regressive intervals of the high-frequency sequences of the Strongoli Sandstone exhibit coarsening- and shallowing-upward trends that are generally more pronounced than those of the high-frequency sequences of the Belvedere Formation. This is evident in the lower part of the Strongoli 3 section (from 0 to 7 m, Figs. 9 and 12), where a rapid transition from relatively distal shoreface deposits containing the LFS and the MFS to hummocky cross-stratified sandstones testifying significant wave energy is documented in only 3 m of succession. A similar situation is partly shown in the upper part of the same section, where transgressive sandstones at ca. 23 m from the base of the section pass into significantly coarser deposits with abundant shell beds and swaley cross-stratification in only 3 m (Fig. 9). In contrast, the coarsening- and shallowing-upward trend in the regressive part of the high-frequency sequence documented in the Strongoli 1 and Strongoli 2 sections is less marked (Figs. 10 and 11).

These observations suggest that the high-frequency sequences of the Strongoli Sandstone could record forced regression in their uppermost part, leading to a rapid bathymetric decrease in response to relative sea-

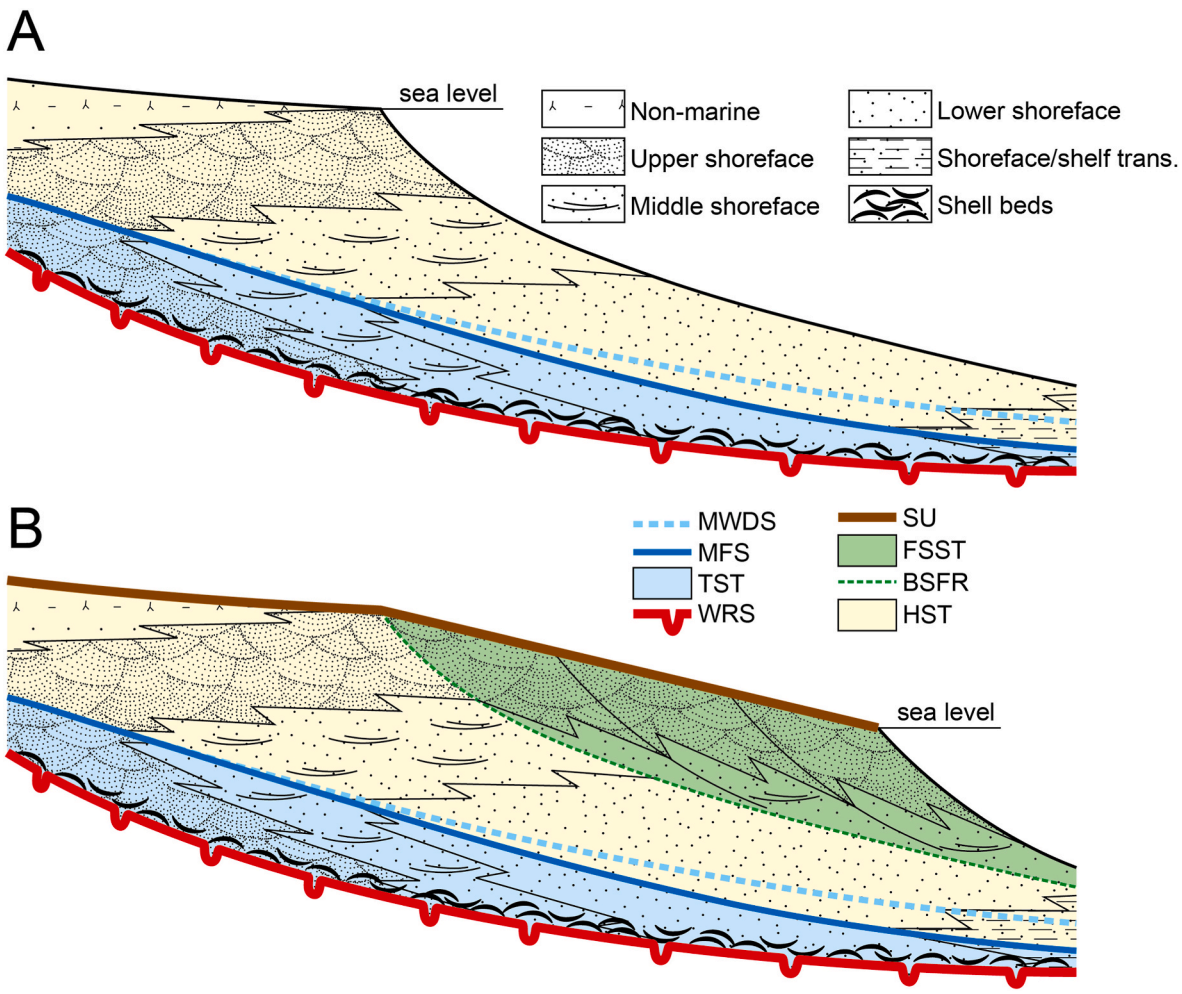

Fig. 15. (A) Typical stratigraphic architecture of the high-frequency sequences of the Zanclean Belvedere Formation (modified from Zecchin et al., 2021). The sequences are bounded by wave ravinement surfaces and are composed of a transgressive systems tract and a highstand systems tract of similar thickness. (B) Typical stratigraphic architecture of the high-frequency sequences of the Gelasian Strongoli Sandstone. The sequences are similar to those of the Belvedere Formation but probably include also forced regressive deposits (see text). Abbreviations: BSFR – basal surface of forced regression; FSST – falling-stage systems tract; HST – highstand systems tract; MFS – maximum flooding surface; MWDS – maximum water depth surface; WRS – wave-ravinement surface; SU – subaerial unconformity; TST – transgressive systems tract.

level fall coupled with sediment accumulation on the seafloor; in this process, the amount of bathymetric reduction exceeds the thickness of the forced regressive sediment that accumulates in proximal settings, adjacent to the shoreline (Posamentier and Allen, 1999). This interpretation is tentative because of the uncertainty surrounding the paleobathymetric reconstructions from the fossil record, as well as because a regressive surface of marine erosion (RSME; Plint, 1988; Plint and Nummedal, 2000), juxtaposing proximal and distal deposits, has not been observed. The latter might be justified by the relatively proximal position of the sections, which consist of fully shoreface deposits (Catuneanu, 2006). Another clue about a more pronounced regressive trend in the high-frequency sequences of the Strongoli Sandstone is provided by the observation that the decreasing trend of the D/P parameter after its peak is on average stronger compared to that observed in most of the high-frequency sequences of the Belvedere Formation (Figs. 5–8 and 10-13).

7. Discussion

The integration of sedimentological and micropaleontological data is very effective in recognizing transgressive and regressive trends, as well as in estimating the position of the MFS, DLS, LFS and MWDS, in the high-frequency stratigraphic sequences composing the Zanclean Belvedere Formation and the Gelasian Strongoli Sandstone of the Crotone Basin. Given their similar facies and stratigraphic architectures, consisting of shell-rich and siliciclastic shoreface deposits forming transgressive and regressive intervals of comparable thickness (T-R cycle architecture of Zecchin, 2007) (Figs. 5–8 and 10-13), the high-frequency sequences of the Belvedere and Strongoli formations probably accumulated under similar conditions and underlying controls, leading to limited shoreline shifts. These analogies contrast with the different settings in which the two units accumulated, as the Belvedere Formation represents the infill of half-graben sub-basins controlled by synsedimentary normal faults and shows a pronounced aggradational component (Zecchin et al., 2006), whereas the Strongoli Sandstone exhibits a marked progradation. Therefore, the common underlying control may relate to the climatic regime rather than the tectonic setting.

Overall, the features of the studied high-frequency sequences fit with those characterizing glacio-eustatic sequences during Icehouse periods (i.e., Late Carboniferous/Early Permian, Oligo-Miocene, and Plio-Pleistocene); in particular, a relatively small thickness (few meters to few decameters), erosional truncation at the top, incomplete systems tract development, and relatively thick transgressive deposits (T and T-R cycle architectures) are typical features in such contexts (e.g., Naish and Kamp, 1997a; Saul et al., 1999; Fielding et al., 2006; Cantalamessa et al., 2007; Di Celma and Cantalamessa, 2007; Zecchin, 2007; Zecchin et al.,

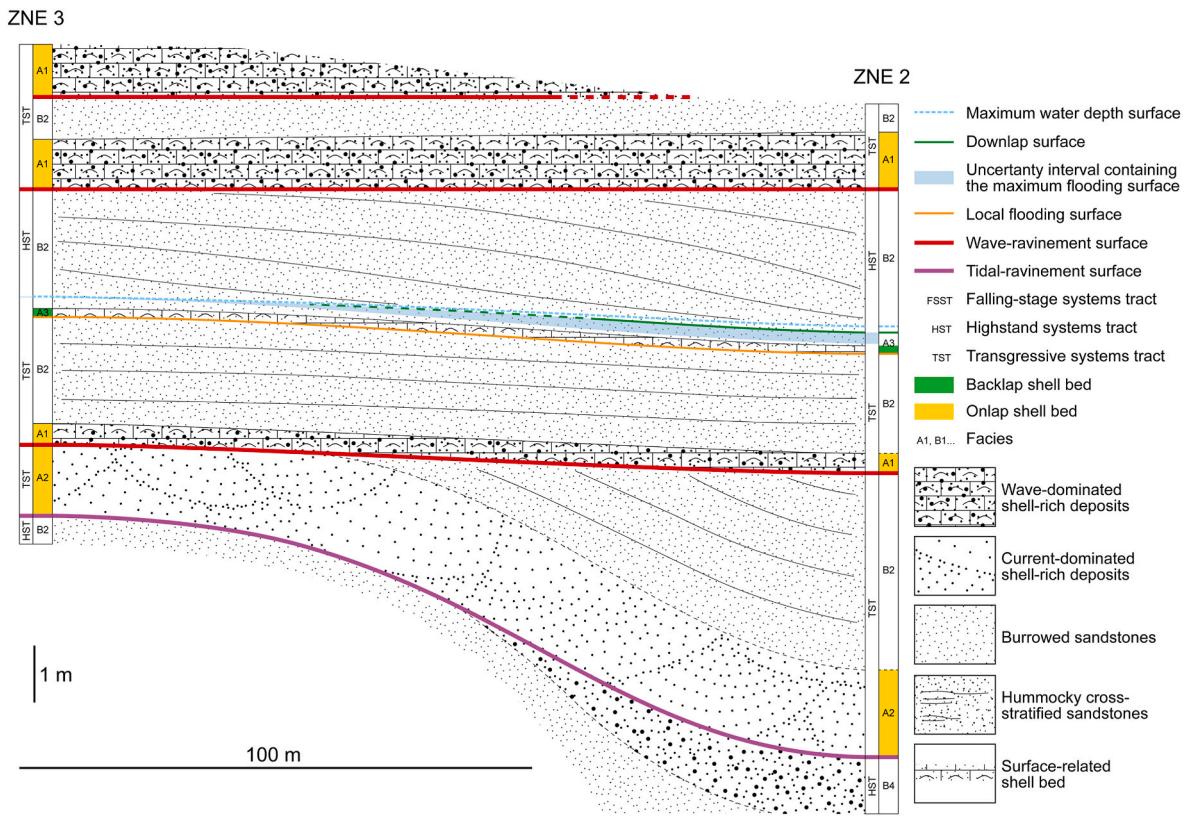

Fig. 16. Correlation of the ZNE 2 and ZNE 3 sections of the Belvedere Formation (Fig. 1D for location), which document the same high-frequency sequences. Deeper depositional settings are toward the right. Note the deep truncation of the lower sequence at the ZNE 3 section and the symmetric architecture of the overlying sequence, which is composed of a TST and a HST of similar thickness. A backlap shell bed lies in the middle of the sequence.

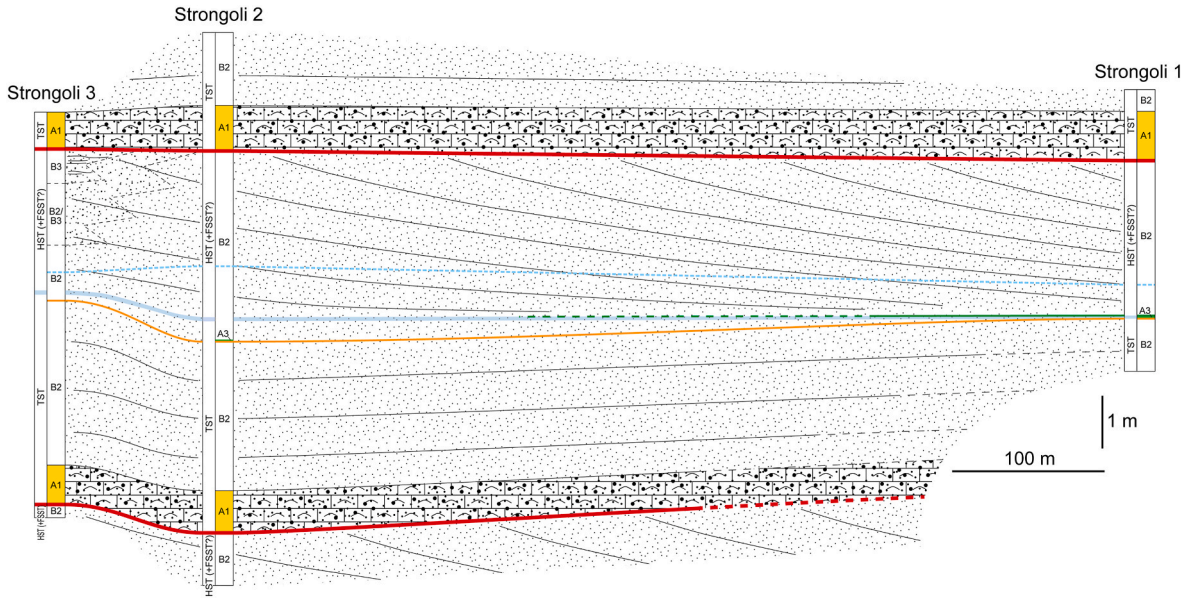

Fig. 17. Correlation of the Strongoli 1 and Strongoli 2 sections and the lower part of the Strongoli 3 section of the Strongoli Sandstone (Fig. 1C for location and Fig. 16 for symbols), which document the same high-frequency sequence. Deeper depositional settings are toward the right. Note the symmetric architecture of the sequence, which is composed of a TST and a HST (probably plus a FSST) of similar thickness.

2021, 2022).

A correlation between the high-frequency cyclicity of the Belvedere Formation and the Milankovitch cyclicity, in particular the 22 kyr duration of precession cycles, was already proposed by Zecchin (2005) and Zecchin et al. (2017); in fact the lack of FSST deposits in the high-frequency sequences (Fig. 15A) fits well with a control mechanism consisting of alternating dry/wet phases and related sediment supply changes which typified the precession-driven cyclicity during the Zanclean (Hilgen and Langereis, 1989; Hilgen, 1991; Roveri and Taviani, 2003; Ochoa et al., 2018). As a result, the inferred precession-paced

sediment supply changes would have resulted in alternating TSTs and HSTs, which reflected dry and wet phases, respectively (Zecchin et al., 2017). In particular, drier periods would have caused a decrease in the terrigenous input to the basin and favored the carbonate factory, as observed in the TSTs of the high-frequency sequences of the Belvedere Formation, whereas the opposite occurred during wet periods (Zecchin et al., 2017). Eventual minor glacio-eustatic sea-level falls were probably counteracted by fault-controlled subsidence in the half-graben sub-basins of the Belvedere Formation, resulting in continuous relative sea-level rise with variable rates and the absence of FSST and LST deposits (Fig. 15A). Considering the recognized number of high-frequency sequences (30–35) and the inferred precession control, the overall duration for the accumulation of the Belvedere Formation would range between 660 and 770 kyr, which is realistic.

The similarity between the high-frequency sequences of the Belvedere Formation and those of the Strongoli Sandstone suggests that a Milankovitch control with marked climatic signature may also be inferred for the latter. In particular, a 41-kyr period, obliquity-paced glacio-eustatic cyclicity is known for the latest Piacenzian and Gelasian times since ca. 2.8–2.7 Ma (Lisiecki and Raymo, 2005; Grant et al., 2018, 2019; Ochoa et al., 2018), during which the Strongoli Sandstone accumulated. A climate-driven cyclicity is also suggested by the cyclic variability of the sea surface temperature (SST) parameter calculated by Capraro et al. (2006) by means of planktonic foraminifera in the Cutro Clay just below the Strongoli Sandstone (Fig. 4A). Given that six high-frequency sequences were recognized in the Strongoli Sandstone (Fig. 9), and considering an obliquity control, a duration of ca. 250 kyr for the accumulation of the unit is inferred.

Since the Gelasian obliquity-paced cyclicity was associated with relatively modest glacio-eustatic sea-level changes (Naish and Wilson, 2009; Grant et al., 2019), this may explain the inferred stages of relative sea-level fall in the upper part of the high-frequency sequences of the Strongoli Sandstone (Section 6.2), a feature that differentiates these sequences from those of the Belvedere Formation (Fig. 15A and B).

The similar thickness of the high-frequency sequences of the Strongoli Sandstone and of the Belvedere Formation, despite the inferred different Milankovitch periodicities, would therefore be coincidental, due to different subsidence and sedimentation rates. In particular, the subsidence in the half-graben sub-basins in which the Belvedere Formation accumulated led to an increase in the thickness of the high-frequency sequences and the suppression of relative sea-level fall; in contrast, subsidence rates would have been lower during the accumulation of the Strongoli Sandstone, resulting in Gelasian obliquity-driven sequences of comparable thickness to the Zanclean precession-driven sequences of the Belvedere Formation.

The high-frequency sequences of the Strongoli Sandstone are time-equivalent with part of the sedimentary succession of the Wanganui Basin, New Zealand, where spectacular obliquity-driven high-frequency sequences were documented (Naish and Kamp, 1997a; Saul et al., 1999; Grant et al., 2018, 2019). The New Zealand high-frequency sequences are on average about 50 m thick, implying radically different subsidence and sedimentation rates with respect to the Crotone Basin, and also show a more marked facies and environmental variability, although OSBs and BSBs are well recognizable in both contexts. Higher basin subsidence, accompanied by an adequately high sediment supply, probably favored the accumulation of relatively thicker sequences, as well as deeper depositional settings toward maximum flooding conditions in the Wanganui Basin, compared to the Crotone example. From both an architectural standpoint and recorded thicknesses, the high-frequency sequences of the Strongoli Sandstone, as well as those of the Belvedere Formation, are closer to the Pleistocene high-frequency sequences of the Canoa Basin (Ecuador) (Di Celma et al., 2005).

Similarly to the lower to middle Pleistocene succession of the SW part of the Crotone Basin, documenting a glacio-eustatic cyclicity in the shallow-marine to continental San Mauro Sandstone (Massari et al., 1999, 2002, 2007), the Zanclean and Gelasian successions appear to be critical for the study of the shallow-water counterpart of the Milankovitch cyclicity, already known in deep-water settings (Hilgen and Langereis, 1989; Hilgen, 1991; Roveri and Taviani, 2003; Ochoa et al., 2018). Further studies are necessary to better link the shallow- and deep-water cyclicity in order to achieve a reliable geological history in any depositional context and a better definition of the timing of depositional and erosional events in sedimentary basins.

8. Conclusions

The high-frequency sequences of the Zanclean Belvedere Formation and the Gelasian Strongoli Sandstone of the Crotone Basin share several features, in particular similar thicknesses (less than 10 m), modest facies changes mainly represented by lower shoreface deposits, onlap shell beds above the basal ravinement surface, and a symmetric stratigraphic architecture consisting of transgressive and regressive deposits of similar thickness. The features of these high-frequency sequences, which remain the same despite the different tectonic settings in which the two units accumulated, suggest a common underlying control by climate and sediment supply changes, as well as minor relative sea-level changes, tuned by the Milankovitch cyclicity. In particular, the 22 kyr duration precession cyclicity and the 41 kyr duration obliquity cyclicity are well known for the Zanclean and Gelasian, respectively, during which the studied successions accumulated. Different subsidence and sedimentation rates (inferred to be higher for the Belvedere Formation) led to the accumulation of high-frequency sequences of similar thickness despite the different dominant periodicities during Zanclean and Gelasian times.

The Belvedere and Strongoli formations, therefore, are inferred to represent the shallow-water equivalents of the well-known Milankovitch cycles documented in the deep-water record, and their study is critical to better understand the relationships between climate, sea-level change, and sedimentation during the Neogene.

CRediT authorship contribution statement

Massimo Zecchin: Writing – review & editing, Writing – original draft, Visualization, Supervision, Methodology, Investigation, Formal analysis, Conceptualization. **Mauro Caffau:** Methodology, Investigation, Formal analysis, Data curation. **Octavian Catuneanu:** Writing – review & editing, Investigation.

Declaration of competing interest

The authors declare that they have no known competing financial interests or personal relationships that could have appeared to influence the work reported in this paper.

Data availability

Data will be made available on request.

Acknowledgments

We thank Salvatore Critelli, an anonymous reviewer and the Editor Istvan Csato for helpful and constructive comments during the review process.

Appendix A. Supplementary data

Supplementary data to this article can be found online at https://doi.org/10.1016/j.marpetgeo.2024.106753.

References

Abbott, S.T., Carter, R.M., 1994. The sequence architecture of Mid-Pleistocene (c.1.1.-0.4Ma) cyclothems from New Zealand: facies development during a Period of orbital

control on sea-level cyclicity. In: De Boer, P.L., Smith, D.G. (Eds.), Orbital Forcing and Cyclic Sequences, vol. 19. IAS Special Publication, pp. 367–394.
Abbott, S.T., 1997. Foraminiferal paleobathymetry and mid-cycle architecture of mid-Pleistocene depositional sequences, Wanganui Basin, New Zealand. Palaios 12, 267–281.
Allen, G.P., Posamentier, H.W., 1993. Sequence stratigraphy and facies model of an incised valley fill: the Gironde estuary, France. J. Sediment. Petrol. 63, 378–391.
Amodio Morelli, L., Bonardi, G., Colonna, V., Dietrich, D., Giunta, G., Ippolito, F., Liguori, V., Lorenzoni, S., Paglionico, A., Perrone, V., Picarretta, G., Russo, M., Scandone, P., Zanettin-Lorenzoni, E., Zuppetta, A., 1976. L'Arco Calabro-Peloritano nell'orogene Appenninico-Maghrebide. Memor. Soc. Geol. Ital. 17, 1–60.
Bonardi, G., Cavazza, W., Perrone, V., Rossi, S., 2001. Calabria–peloritani terrane and northern Ionian sea. In: Vai, G.B., Martini, I.P. (Eds.), Anatomy of an Orogen: the Apennines and Adjacent Mediterranean Basins. Kluwer Academic Publishers, Bodmin, pp. 287–306.
Cantalamessa, G., Di Celma, C., Ragaini, L., 2005. Sequence stratigraphy of the Punta Ballena Member of the Jama Formation (Early Pleistocene, Ecuador): insights from integrated sedimentologic, taphonomic and paleoecologic analysis of molluscan shell concentrations. Palaeogeogr. Palaeoclimatol. Palaeoecol. 216, 1–25.
Cantalamessa, G., Di Celma, C., Ragaini, L., Valleri, G., Landini, W., 2007. Sedimentology and high-resolution sequence stratigraphy of the late middle to late Miocene Angostura Formation (western Borbón Basin, northwestern Ecuador). Journal of the Geological Society of London 164, 653–665.
Capraro, L., Consolaro, C., Fornaciari, E., Massari, F., Rio, D., 2006. Chronology of the middle-upper Pliocene succession in the Strongoli area: constraints on the geological evolution of the Crotone Basin (southern Italy). In: Moratti, G., Chalouan, A. (Eds.), Tectonics of theWestern Mediterranean and North Africa, vol. 262. Geological Society Special Publication, pp. 323–336.
Carter, R.M., Fulthorpe, C.S., Naish, T.R., 1998. Sequence concepts at seismic and outcrop scale: the distinction between physical and conceptual stratigraphic surfaces. Sediment. Geol. 122, 165–179.
Catuneanu, O., 2006. Principles of Sequence Stratigraphy. Elsevier, Amsterdam, p. 386.
Catuneanu, O., 2019. Scale in sequence stratigraphy. Mar. Petrol. Geol. 106, 128–159.
Catuneanu, O., 2022. Principles of Sequence Stratigraphy, second ed. Elsevier, Amsterdam, p. 494.
Catuneanu, O., Zecchin, M., 2013. High-resolution sequence stratigraphy of clastic shelves II: controls on sequence development. Mar. Petrol. Geol. 39, 26–38.
Cita, M.B., 1975. Studi sul Pliocene e sugli strati di passaggio dal Miocene al Pliocene. VIII. Planktonic foraminiferal biozonation of the Mediterranean Pliocene deep-sea record. A revision. Riv. Ital. Paleontol. Stratigr. 81, 527–544.
Clifton, H.E., 2006. A Reexamination of facies Models for clastic shorelines. In: Posamentier, H.W., Walker, R.G. (Eds.), Facies Models Revisited, vol. 84. SEPM Special Publication, pp. 293–337.
Criniti, S., Borrelli, M., Falsetta, E., Civitelli, M., Pugliese, E., Arcuri, N., 2023. Sandstone petrology of the Crotone basin, Calabria (Italy) from well cores. Rendiconti Online della Società Geologica Italiana 59. https://doi.org/10.3301/ROL.2023.10.
Critelli, S., 2018. Provenance of Mesozoic to Cenozoic Circum-Mediterranean sandstones in relation to tectonic setting. Earth Sci. Rev. 185, 624–648.
Critelli, S., Martín-Martín, M., 2022. Provenance, Paleogeographic and paleotectonic interpretations of Oligocene-Lower Miocene sandstones of the western-central Mediterranean region: a review. J. Asian Earth Sci. X 8, 100124. https://doi.org/10.1016/j.jaesx.2022.100124.
Critelli, S., Martín-Martín, M., 2024. History of western Tethys Ocean and the birth of the circum-Mediterranean orogeny as reflected by source-to-sink relations. Int. Geol. Rev. 66, 505–515.
Di Celma, C., Ragaini, L., Cantalamessa, G., Landini, W., 2005. Basin physiography and tectonic influence on the sequence architecture and stacking pattern: Pleistocene succession of the Canoa Basin (central Ecuador). GSA Bulletin 117, 1226–1241.
Di Celma, C., Cantalamessa, G., 2007. Sedimentology and high-frequency sequence stratigraphy of a forearc extensional basin: the Miocene Caleta Herradura Formation, Mejillones Peninsula, northern Chile. Sediment. Geol. 198, 29–52.
Donnici, S., Serandrei-Barbero, R., 2002. The benthic foraminiferal communities of the North Adriatic continental shelf. Mar. Micropaleontol. 44, 93–123.
Dott, R.H., Bourgeois, J., 1982. Hummocky stratification: significance of its variable bedding sequences. GSA Bulletin 93, 663–680.
Dumas, S., Arnott, R.W.C., Southard, J.B., 2005. Experiments on oscillatory-flow and combined-flow bed forms: implications for interpreting parts of the shallow-marine sedimentary record. J. Sediment. Res. 75, 501–513.
Embry, A.F., Johannessen, E.P., 1992. T-R sequence stratigraphy, facies analysis and reservoir distribution in the uppermost Triassic–Lower Jurassic succession, Western Sverdrup Basin, Arctic Canada. In: Vorren, T.O., Bergsager, E., Dahl-Stamnes, O.A., Holter, E., Johansen, B., Lie, E., Lund, T.B. (Eds.), Arctic Geology and Petroleum Potential, vol. 2. Norwegian Petroleum Society Special Publication, pp. 121–146.
Faccenna, C., Becker, T.W., Lucente, F.P., Jolivet, L., Rossetti, F., 2001. History of subduction and back-arc extension in the Central Mediterranean. Geophys. J. Int. 145, 809–820.
Faccenna, C., Civetta, L., D'Antonio, M., Funiciello, F., Margheriti, L., Piromallo, C., 2005. Constraints on mantle circulation around the deforming Calabrian slab. Geophys. Res. Lett. 32, L06311 https://doi.org/10.1029/2004GL021874.
Fielding, C.R., Bann, K.L., MacEachern, J.A., Stuart, C.T., Jones, B.G., 2006. Cyclicity in the nearshore marine to coastal, Lower Permian, Pebbley Beach Formation, southern Sydney Basin, Australia: a record of relative sea-level fluctuations at the close of the Late Palaeozoic Gondwanan ice age. Sedimentology 53, 435–463.
Fillon, R.H., 2007. Biostratigraphy and condensed sections in deepwater settings. In: Weimer, P., Slatt, R. (Eds.), Introduction to the Petroleum Geology of Deepwater Settings, AAPG Studies in Geology 57, AAPG/Datapages Discovery Series 8.
Fürsich, F.T., Oschmann, W., 1993. Shell beds as tools in basin analysis: the Jurassic of Kachchh, western India. J. Geol. Soc. 150, 169–185. London.
Fürsich, F.T., Pandey, P.K., 1999. Genesis and environmental significance of Upper Cretaceous shell concentrations from the Cauvery Basin, southern India. Palaeogeogr. Palaeoclimatol. Palaeoecol. 145, 119–139.
Galloway, W.E., Hobday, D.K., 1996. Terrigenous Clastic Depositional Systems - Applications to Fossil Fuel and Groundwater Resources, second ed. Springer, New York, p. 489.
Grant, G.R., Sefton, J.P., Patterson, M.O., Naish, T.R., Dunbar, G.B., Hayward, B.W., Morgans, H.E.G., Alloway, B.V., Seward, D., Tapia, C.A., Prebble, J.G., Kamp, P.J.J., McKay, R., Ohneiser, C., Turner, G.M., 2018. Mid- to late Pliocene (3.3–2.6 Ma) global sea-level fluctuations recorded on a continental shelf transect, Whanganui Basin, New Zealand. Quat. Sci. Rev. 201, 241–260.
Grant, G.R., Naish, T.R., Dunbar, G.B., Stocchi, P., Kominz, M.A., Kamp, P.J.J., Tapia, C. A., McKay, R.M., Levy, R.H., Patterson, M.O., 2019. The amplitude and origin of sea-level variability during the Pliocene epoch. Nature 574, 237–241. https://doi.org/10.1038/s41586-019-1619-z.
Guillaume, B., Funiciello, F., Faccenna, C., Martinod, J., Olivetti, V., 2010. Spreading pulses of the Tyrrhenian sea during the narrowing of the Calabrian slab. Geology 38, 819–822.
Gutiérrez Paredes, H.C., Catuneanu, O., Romano, U.H., 2017. Sequence stratigraphy of the Miocene section, southern Gulf of Mexico. Mar. Petrol. Geol. 86, 711–732.
Hart, B.S., Plint, A.G., 1995. Gravelly shoreface and beachface deposits. In: Plint, A.G. (Ed.), Sedimentary Facies Analysis, vol. 22. International Association of Sedimentologists Special Publication, pp. 75–99.
Hilgen, F.J., 1991. Extension of the astronomically calibrated (polarity) to the Miocene/Pliocene boundary. Earth Planet Sci. Lett. 107, 349–368.
Hilgen, F.J., Langereis, C.G., 1989. Periodicities of $CaCO_3$ cycles in the Pliocene of Sicily: discrepancies with the quasi-periods of the Earth's orbital cycles? Terra. Nova 1, 409–415.
Johnson, J.G., Murphy, M.A., 1984. Time-rock model for Siluro-Devonian continental shelf, western United States. GSA Bulletin 95, 1349–1359.
Kidwell, S.M., 1991. Condensed deposits in siliciclastic sequences: expected and observed features. In: Einsele, G., Ricken, W., Seilacher, A. (Eds.), Cycles and Events in Stratigraphy. Springer-Verlag, Berlin, pp. 682–695.
Kidwell, S.M., Fürsich, F.T., Aigner, T., 1986. Conceptual framework for the analysis and classification of fossil concentrations. Palaios 1, 228–238.
Kondo, Y., Abbott, S.T., Kitamura, A., Kamp, P.J.J., Naish, T.R., Kamataki, T., Saul, G.S., 1998. The relationship between shell bed type and sequence architecture: examples from Japan and New Zealand. Sediment. Geol. 122, 109–127.
Leckie, D.A., Walker, R.G., 1982. Storm- and tide-dominated shorelines in Cretaceous Moosebar-Lower Gates interval-outcrop equivalents of deep basin gas trap in Western Canada. AAPG (Am. Assoc. Pet. Geol.) Bull. 66, 138–157.
Lisiecki, L.E., Raymo, M.E., 2005. A Pliocene-Pleistocene stack of 57 globally distributed benthic δ18O records. Paleoceanography 20, PA1003. https://doi.org/10.1029/2004PA001071.
Loeblich, A.R., Tappan, H., 1987. Foraminiferal Genera and Their Classification. Van Nostrand Reinhold Company, New York, p. 970.
Longhitano, S.G., Chiarella, D., Di Stefano, A., Messina, C., Sabato, L., Tropeano, M., 2012. Tidal signatures in Neogene to Quaternary mixed deposits of southern Italy straits and bays. Sediment. Geol. 279, 74–96.
Lourens, L.J., Antonarakou, A., Hilgen, F.J., Van Hoof, A.A.M., Vergnaud-Grazzini, C., Zachariasse, W.J., 1996. Evaluation of the Plio-Pleistocene astronomical timescale. Paleoceanography 11, 391–413.
Malinverno, A., Ryan, W.B.F., 1986. Extension in the Tyrrhenian Sea and shortening in the Apennines as a result of arc migration driven by sinking of the lithosphere. Tectonics 5, 227–245.
Massari, F., Parea, G.C., 1988. Progradational gravel beach sequences in a moderate- to high-energy, microtidal marine environment. Sedimentology 35, 881–913.
Massari, F., Sgavetti, M., Rio, D., D'Alessandro, A., Prosser, G., 1999. Sedimentary record of falling stages of Pleistocene glacio-eustatic cycles in shelf setting (Crotone basin, south Italy). Sediment. Geol. 127, 85–110.
Massari, F., Rio, D., Sgavetti, M., Prosser, G., D'alessandro, A., Asioli, A., Capraro, L., Fornaciari, E., Tateo, F., 2002. Interplay between tectonics and glacio-eustasy: Pleistocene succession of the Crotone basin, Calabria (southern Italy). GSA Bulletin 114, 1183–1209.
Massari, F., Capraro, L., Rio, D., 2007. Climatic modulation of timing of systems-tract development with respect to sea-level changes (middle Pleistocene of Crotone, Calabria, Southern Italy). J. Sediment. Res. 77, 461–468.
Massari, F., Prosser, G., 2013. Late Cenozoic tectono-stratigraphic sequences of the Crotone Basin: insights on the geodynamic history of the Calabrian Arc and Tyrrhenian sea. Basin Res. 25, 26–51.
Meldahl, K.H., 1993. Geographic gradients in the formation of the shell concentrations: Plio-Pleistocene marine deposits Gulf of California. Palaeogeogr. Palaeoclimatol. Palaeoecol. 101, 1–25.
Mendes, I., Gonzalez, R., Dias, J.M.A., Lobo, F., Martins, V., 2004. Factors influencing recent benthic foraminifera distribution on the Guadiana shelf (Southwestern Iberia). Mar. Micropaleontol. 51, 171–192.
Morigi, C., Jorissen, F.J., Fraticelli, S., Horton, B.P., Principi, M., Sabbatini, A., Capotondi, L., Curzi, P.V., Negri, A., 2005. Benthic foraminiferal evidence for the formation of the Holocene mud-belt and bathymetrical evolution in the central Adriatic Sea. Mar. Micropaleontol. 57, 25–49.
Naish, T.R., Kamp, P.J.J., 1997a. Sequence stratigraphy of sixth-order (41 k.y.) Pliocene–Pleistocene cyclothems, Wanganui basin, New Zealand: a case for the regressive systems tract. GSA Bulletin 109, 978–999.

Naish, T.R., Kamp, P.J.J., 1997b. Foraminiferal depth palaeoecology of Late Pliocene shelf sequences and system tracts, Wanganui Basin, New Zealand. Sediment. Geol. 110, 237–255.
Naish, T.R., Wilson, G.S., 2009. Constraints on the amplitude of Mid-Pliocene (3.6–2.4 Ma) eustatic sea-level fluctuations from the New Zealand shallow-marine sediment record. Philosophical Transactions of the Royal Society A 367, 169–187.
Norris, R.D., 1986. Taphonomic gradients in shelf fossil assemblages: Pliocene Purisima Formation. Palaios 1, 256–270. California.
Ochoa, D., Sierro, F.J., Hilgen, F.J., Cortina, A., Lofi, J., Kouwenhoven, T., Flores, J.-A., 2018. Origin and implications of orbital-induced sedimentary cyclicity in Pliocene well-logs of the Western Mediterranean. Mar. Geol. 403, 150–164.
Phipps, M.D., Kaminiski, M.A., Aksu, A.E., 2010. Calcareous benthic foraminiferal biofacies along a depth transect on the southwestern marmara shelf (Turkey). Micropaleontology 56, 377–392.
Plint, A.G., 1988. Sharp-based shoreface sequences and offshore bars in the Cardium Formation of Alberta; their relationship to relative changes in sea level. In: Wilgus, C.K., Hastings, B.S., Kendall, C.G.StC., Posamentier, H.W., Ross, C.A., Van Wagoner, J.C. (Eds.), Sea Level Changes: an Integrated Approach, vol. 42. SEPM Special Publication, pp. 357–370.
Plint, A.G., Nummedal, D., 2000. The falling stage systems tract: recognition and importance in sequence stratigraphic analysis. In: Hunt, D., Gawthorpe, R.L. (Eds.), Sedimentary Responses to Forced Regressions, vol. 172. Geological Society Special Publication, pp. 1–17.
Posamentier, H.W., Allen, G.P., 1999. Siliciclastic sequence stratigraphy – concepts and applications. SEPM Concepts in Sedimentology and Paleontology 7, 210.
Raffi, I., Backman, J., Fornaciari, E., Pálike, H., Rio, D., Lourens, L., Hilgen, F., 2006. A review of calcareous nannofossil astrobiochronology encompassing the past 25 million years. Quat. Sci. Rev. 25, 3113–3137.
Reading, H.G., Collinson, J.D., 1996. Clastic Coasts. In: Reading, H.G. (Ed.), Sedimentary Environments; Processes, Facies and Stratigraphy. Blackwell Science, Oxford, pp. 154–231.
Rio, D., Raffi, I., Villa, G., 1990. Pliocene-Pleistocene calcareous nannofossil distribution patterns in the Western Mediterranean. In: Kastens, K.A., Mascle, J. (Eds.), Proceedings of the ODP, Scientific Results, pp. 513–533, 107.
Roda, C., 1964. Distribuzione e facies dei sedimenti Neogenici nel Bacino Crotonese. Geol. Rom. 3, 319–366.
Roveri, M., Taviani, M., 2003. Calcarenite and sapropel deposition in the Mediterranean Pliocene: shallow- and deep-water record of astronomically driven climatic events. Terra. Nova 15, 279–286.
Sartori, R., 2003. The Tyrrhenian back-arc basin and subduction of the Ionian lithosphere. Episodes 26, 217–221.
Saul, G., Naish, T.R., Abbott, S.T., Carter, R.M., 1999. Sedimentary Cyclicity in the Marine Pliocene-Pleistocene of the Wanganui Basin (New Zealand): Sequence Stratigraphic Motifs Characteristic of the Past 2.5 m.Y, vol. 111. Geological Society of America Bulletin, pp. 524–537.
Stefanelli, S., 2003. Benthic foraminiferal assemblages as tools for paleoenvironmental reconstruction of the early-middle Pleistocene Motalbano Jonico composite section. Boll. Soc. Paleontol. Ital. 42, 281–299.
Swift, D.J.P., Phillips, S., Thorne, J.A., 1991. Sedimentation on continental margins, IV: lithofacies and depositional systems. In: Swift, D.J.P., Oertel, G.F., Tillman, R.W., Thorne, J.A. (Eds.), Shelf Sand and Sandstone Bodies-Geometry, Facies and Sequence Stratigraphy, vol. 14. IAS Special Publication, pp. 89–152.
Tripodi, V., Muto, F., Brutto, F., Perri, F., Critelli, S., 2018. Neogene-quaternary evolution of the forearc and backarc regions between the Serre and Aspromonte Massifs. Calabria (southern Italy): Mar. Petrol. Geol. 95, 328–343.
Van Dijk, J.P., 1990. Sequence stratigraphy, kinematics and dynamic geohistory of the Crotone Basin (Calabria arc, central mediterranean): an integrated approach. Memor. Soc. Geol. Ital. 44, 259–285.
Van Dijk, J.P., Okkes, F.W.M., 1991. Neogene tectonostratigraphy and kinematics of Calabrian basins; implications for the geodynamics of the Central Mediterranean. Tectonophysics 196, 23–60.
Van Dijk, J.P., Bello, M., Brancaleoni, G.P., Cantarella, G., Costa, V., Frixa, A., Golfetto, F., Merlini, S., Riva, M., Torricelli, S., Toscano, C., Zerilli, A., 2000. A regional structural model for the northern sector of the Calabrian Arc (southern Italy). Tectonophysics 324, 267–320.
Van Wagoner, J.C., Posamentier, H.W., Mitchum, R.M., Vail, P.R., Sarg, J.F., Loutit, T.S., Hardenbol, J., 1988. An overview of the fundamentals of sequence stratigraphy and key definitions. In: Wilgus, C.K., Hastings, B.S., Kendall, C.G.StC., Posamentier, H. W., Ross, C.A., Van Wagoner, J.C. (Eds.), Sea Level Changes: an Integrated Approach, vol. 42. SEPM Special Publication, pp. 39–45.
Van Wagoner, J.C., Mitchum, R.M., Campion, K.M., Rahmanian, V.D., 1990. Siliciclastic sequence stratigraphy in well logs, cores, and outcrops. AAPG Methods in Exploration 7, 55.
Zecchin, M., 2005. Relationships between fault-controlled subsidence and preservation of shallow-marine small-scale cycles: example from the lower Pliocene of the Crotone Basin (southern Italy). J. Sediment. Res. 75, 300–312.
Zecchin, M., 2007. The architectural variability of small-scale cycles in shelf and ramp clastic systems: the controlling factors. Earth Sci. Rev. 84, 21–55.
Zecchin, M., Caffau, M., 2012. The vertical compartmentalization of reservoirs: an example from an outcrop analog, Crotone Basin, southern Italy. AAPG (Am. Assoc. Pet. Geol.) Bull. 96, 155–175.
Zecchin, M., Catuneanu, O., 2013. High-resolution sequence stratigraphy of clastic shelves I: units and bounding surfaces. Mar. Petrol. Geol. 39, 1–25.
Zecchin, M., Massari, F., Mellere, D., Prosser, G., 2004. Anatomy and evolution of a mediterranean-type fault bounded basin: the lower pliocene of the northern Crotone Basin (southern Italy). Basin Res. 16, 117–143.
Zecchin, M., Mellere, D., Roda, C., 2006. Sequence stratigraphy and architectural variability in growth fault-bounded basin fills: a review of Plio-Pleistocene stratal units of the Crotone Basin, southern Italy. J. Geol. Soc. 163, 471–486. London.
Zecchin, M., Caffau, M., Ceramicola, S., 2016. Interplay between regional uplift and glacio-eustasy in the Crotone Basin (Calabria, southern Italy) since 0.45 Ma: a review. Global Planet. Change 143, 196–213.
Zecchin, M., Caffau, M., Civile, D., Critelli, S., Di Stefano, A., Maniscalco, R., Muto, F., Sturiale, G., Roda, C., 2012. The Plio-Pleistocene evolution of the Crotone Basin (southern Italy): interplay between sedimentation, tectonics and eustasy in the frame of Calabrian Arc migration. Earth Sci. Rev. 115, 273–303.
Zecchin, M., Caffau, M., Di Stefano, A., Maniscalco, R., Lenaz, D., Civile, D., Muto, F., Critelli, S., 2013a. The Messinian succession of the Crotone Basin (southern Italy) II: facies architecture and stratal surfaces across the Miocene-Pliocene boundary. Mar. Petrol. Geol. 48, 474–492.
Zecchin, M., Civile, D., Caffau, M., Muto, F., Di Stefano, A., Maniscalco, R., Critelli, S., 2013b. The Messinian succession of the Crotone Basin (southern Italy) I: stratigraphic architecture reconstructed by seismic and well data. Mar. Petrol. Geol. 48, 455–473.
Zecchin, M., Praeg, D., Ceramicola, S., Muto, F., 2015. Onshore to offshore correlation of regional unconformities in the Plio-Pleistocene sedimentary successions of the Calabrian Arc (central Mediterranean). Earth Sci. Rev. 142, 60–78.
Zecchin, M., Caffau, M., Catuneanu, O., Lenaz, D., 2017. Discrimination between wave-ravinement surfaces and bedset boundaries in Pliocene shallow-marine deposits, Crotone Basin, southern Italy: an integrated sedimentological, micropaleontological and mineralogical approach. Sedimentology 64, 1755–1791.
Zecchin, M., Catuneanu, O., Caffau, M., 2019. Wave-ravinement surfaces: classification and key characteristics. Earth Sci. Rev. 188, 210–239.
Zecchin, M., Civile, D., Caffau, M., Critelli, S., Muto, F., Mangano, G., Ceramicola, S., 2020. Sedimentary evolution of the Neogene-Quaternary Crotone Basin (southern Italy) and relationships with large-scale tectonics: a sequence stratigraphic approach. Mar. Petrol. Geol. 117, 104381.
Zecchin, M., Caffau, M., Catuneanu, O., 2021. Recognizing maximum flooding surfaces in shallow-water deposits: an integrated sedimentological and micropaleontological approach (Crotone Basin, southern Italy). Mar. Petrol. Geol. 133, 105225.
Zecchin, M., Caffau, M., Catuneanu, O., 2022. Identification of maximum flooding surfaces at different scales: the case of the piacenzian to gelasian Cutro Clay and Strongoli sandstone (Crotone Basin, southern Italy). Mar. Petrol. Geol. 146, 105971.
Zecchin, M., Catuneanu, O., Caffau, M., 2023. High-resolution sequence stratigraphy of clastic shelves IX: methods for recognizing maximum flooding conditions in shallow-marine settings. Mar. Petrol. Geol. 156, 106468.